Received: 9 October 2018 | Revised: 8 May 2019 | Accepted: 14 May 2019

DOI: 10.1111/bre.12373

ORIGINAL ARTICLE

Basin Research | IAS EAGE | WILEY

Drainage reorganization and Laramide tectonics in north-central New Mexico and downstream effects in the Gulf of Mexico

Tyson M. Smith | **Kurt E. Sundell** | **Shelby N. Johnston** | **Carlos N. Guilherme Andrade** | **Ross A. Andrea** | **Jordan N. Dickinson** | **Yiduo A. Liu** | **Michael Andrew Murphy** | **Tom J. Lapen** | **Joel E. Saylor**

Department of Earth and Atmospheric Sciences, University of Houston, Houston, Texas

Correspondence
Tyson M. Smith, Department of Earth and Atmospheric Sciences, University of Houston, Houston, TX.
Email: tysn.smth@gmail.com

Funding information
National Science Foundation, Grant/Award Number: EAR- 1550097 and EAR-1742951; Chevron Corporation

Abstract

The El Rito and Galisteo depocenters in north-central New Mexico archive tectonically-driven Paleogene drainage reorganization, the effects of which influenced sedimentation along the northwestern margin of the Gulf of Mexico. Although separated by ~100 km and lacking depositional chronology for the El Rito Formation, the two aforementioned New Mexican depocenters are commonly considered remnants of a single basin with coeval deposition and shared accommodation mechanism. Detrital zircon U-Pb maximum depositional ages indicate that the El Rito and Galisteo formations are not coeval. Moreover, stratigraphic thickness trends and mapping relationships indicate different accommodation mechanisms for the Galisteo and El Rito depocenters; tectonically-induced subsidence versus infilling of incised topography, respectively. The regional unconformity that bounds the base of both the El Rito and Galisteo formations is a correlative surface induced by local tectonic activity and associated drainage reorganization in the early Eocene, and was diachronously buried by northward onlap of fluvial sediments. Detrital zircon distributions in both depocenters indicate increased recycling of Mesozoic strata above the unconformity, but diverge upsection as topographic prominence of local basement-involved uplifts waned. Sediment capture in these depocenters is coeval with deposition in other externally-drained Laramide basins. Further, it corresponds to a period of low Laramide province-derived sediment input and replacement by Appalachian-sourced sediment along the northwestern margin of the Gulf of Mexico during a basin-wide transgression. This illustrates the potential effect that pockets of sediment storage within the catchment of a transcontinental drainage system can have over the sedimentary record in the receiving marine basin.

KEYWORDS
detrital zircon U-Pb, drainage reorganization, Gulf of Mexico, Laramide, stratigraphy

1 | INTRODUCTION

Drainage reorganization and in-route sediment storage plays a fundamental role in the evolution of source-to-sink depositional systems, and the sedimentary record of those systems preserved in the receiving marine basin (i.e., the ultimate sink; Figure 1). Stream piracy, changes in climate, large-scale tectonic activity, or local changes at the headwaters of rivers can drive changes in sediment routing and storage. Interpretation of the geologic record often depends on accurate identification of drainage reorganization events because they can affect the sediment composition and flux, as well as the isotopic composition of transported sediment (Clift, Blusztajn, & Nguyen, 2006) and water (Davis, Wiegand, Carroll, & Chamberlain, 2008). However, in-route sediment storage may compromise the fidelity of marine records of hinterland activity by altering the sediment character and volume in the ultimate sink (Nie et al., 2015). Therefore, linking specific upstream reorganization events with downstream effects is complicated by large distances, non-unique changes in sediment character, temporary or permanent in-route sediment storage, and poorly understood fluvial pathways.

Intraplate deformation within the Laramide province (Figure 2a) drove local- and continental-scale drainage dynamics through a series of principally internally (i.e., ponded) and externally (i.e., axial and perimeter) drained basins (Dickinson et al., 1988; Lawton, 2008), and was the primary source of sediment in the Gulf of Mexico during the Paleogene (Galloway, Whiteaker, & Ganey-Curry, 2011). Externally draining basins acted as the upstream gatekeepers of clastic material in route to the Gulf of Mexico, sequestering more sediment during periods of increased accommodation and contributing more sediment during periods of bypass and erosion. Details of these upstream controls on downstream depositional processes and products in this continental-scale source-to-sink system remain preliminary, in part due to poor documentation of the evolution of upstream (source) regions.

Highlights

- Recycled Mesozoic detrital zircon populations in north-central New Mexico depocenters, from samples collected above a regional unconformity record exhumation of the Nacimiento Uplift and drainage reorganization.
- Depositional chronology above and below this tectonically-induced, regional unconformity are provided by detrital zircon maximum depositional ages and previously published biostratigraphic data. These age controls clarify the temporal relationship between the northern (El Rito) and southern (Galisteo) depocenters, and timing of local tectonic activity and drainage reorganization.
- Deposition of mid Eocene, uplift-derived sediments in Laramide-style basins and coeval westward infiltration of Appalachian-derived sediments along the Gulf of Mexico margin demonstrate the effect of in-route sediment storage on the distal basin record in cross-continental drainage systems.

We investigate the relationship between the Paleogene drainage reorganization in north-central New Mexico and local tectonic activity. We compare our findings to coeval sedimentation along the northwest margin of the Gulf of Mexico. We interpret early Eocene tectonic activity of the Nacimiento Gallina-Archuleta (NGA) Uplift to be the primary driver of drainage reorganization in our area of focus, the El Rito and Galisteo depocenters (Figures 2 and 3). Spatial variability in unconformity development, stratigraphic architecture, and sediment provenance within the depocenters record the basins' response to this relatively rapid tectonic episode. Sediment provenance in both depocenters indicate an increased recycling of Mesozoic sedimentary strata across this unconformity. However, there is a difference in the duration

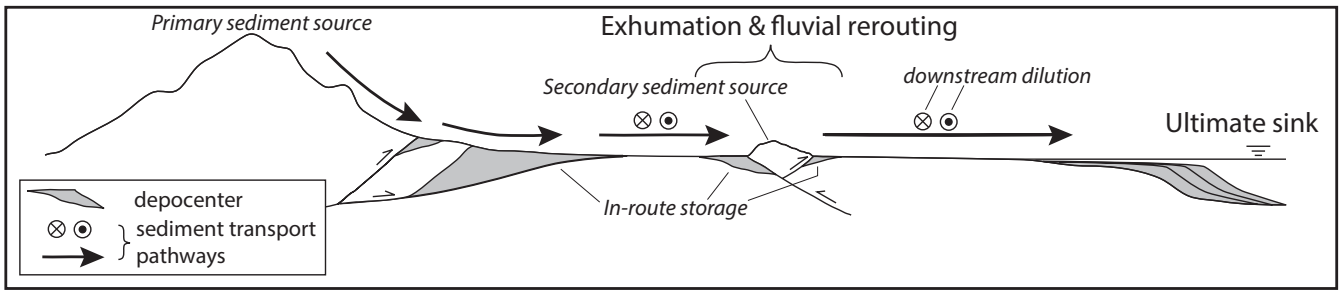

FIGURE 1 Schematic (not to scale) sediment transport pathways (approximately parallel and perpendicular to the down-dip transect) illustrating sources and sinks potentially encountered by transcontinental river systems. In-route storage and secondary source contribution of sediment can affect sediment character and volume while downstream dilution obscures sediment source signals through fluvial integration in the receiving marine basin (i.e., ultimate sink)

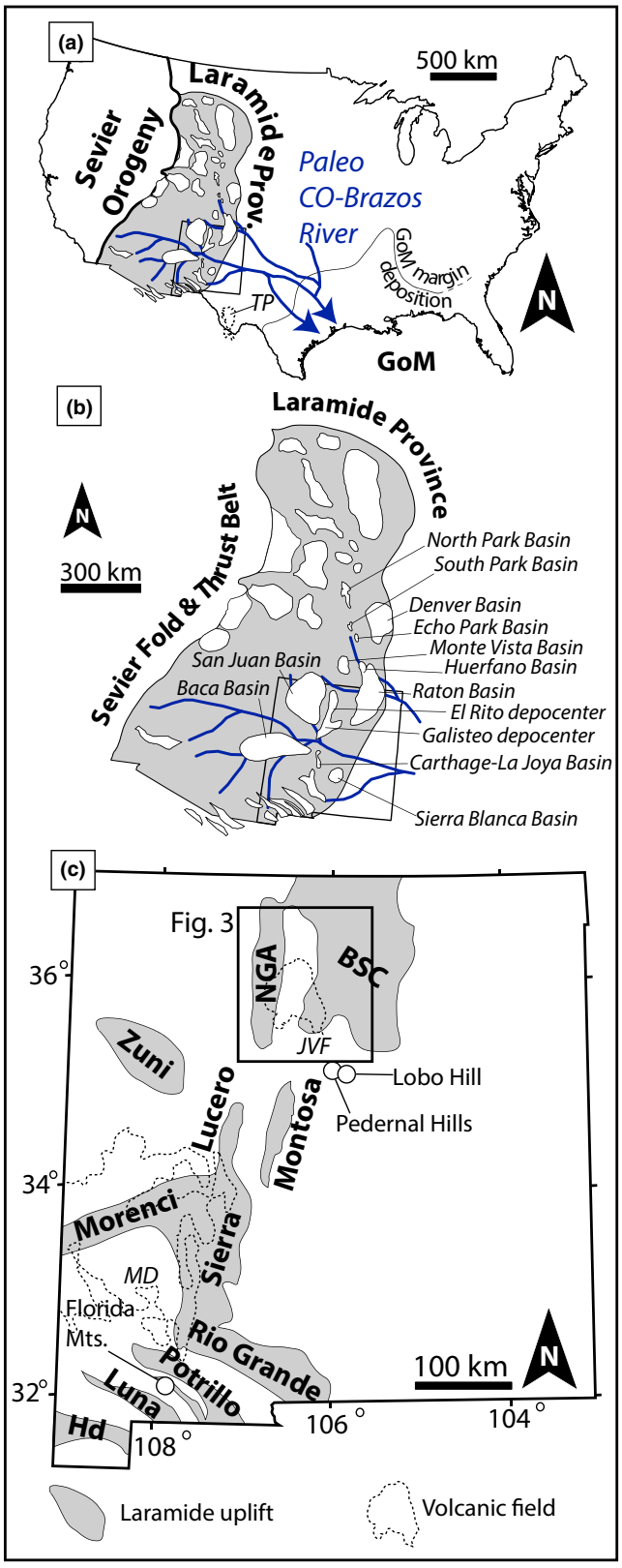

FIGURE 2 (a) Map of North America showing the boundary between the Sevier Orogeny (Weil & Yonkee, 2012) and the Laramide province (Lawton, 2008; Weil & Yonkee, 2012), proposed late Paleocene–early Eocene paleo Colorado Brazos River system (Blum et al., 2017), Gulf of Mexico (GoM), and New Mexico. The inland extent of early Eocene GoM margin deposition (Galloway et al., 2011) is labelled as such and indicated by a thin solid black line that becomes dashed at the eastern end. Tp-Trans Pecos volcanic field, CO-Colorado. (b) Map of Laramide province from Figure 2a with headwaters of the Colorado-Brazos River system in Figure 2a, Laramide basins (adapted from Lawton, 2008), and labelled basins discussed in paper. (c) Map of New Mexico showing Laramide uplifts (adapted from Averill & Miller, 2013; Cather, 2004; Clinkscales & Lawton, 2015) and Cenozoic volcanic fields (Hudson & Grauch, 2013). The box indicates location of Figure 3. BSC, Brazos-Sangre de Cristo; Hd, Hildago; JVF, Jemez volcanic field; MD, Mogollon-Datil volcanic field; Mts., mountains; NGA, Nacimiento-Gallina-Archuleta

of unconformity development and a divergent evolution of sediment provenance following the initial phase of increased recycled Mesozoic strata between the two depocenters. Periods of erosion within the Galisteo depocenter, as well as other externally draining basins (Dickinson et al., 1988) contained within the Colorado-Brazos River catchment (Blum et al., 2017), correspond to enhanced sedimentation rates in the Gulf of Mexico (Galloway et al., 2011). Conversely, during waning tectonic activity and sediment capture in the Galisteo depocenter areas as well as other Laramide basins, resulting sediment volumes greatly decreased along the Gulf of Mexico margin (Galloway et al., 2011), which enabled westward infiltration of Appalachian-derived sediment into the distal reaches of the Colorado-Brazos River system during the middle Eocene. Synthesis of previous work and new data presented herein record the tectonic activity and basin development driving hinterland drainage reorganization of primary and secondary rivers within a long-lived continental scale drainage system.

2 | GEOLOGIC BACKGROUND

2.1 | Geologic setting

The North American western interior experienced a fundamental shift in deformation style and sedimentation during the Late Cretaceous–Paleogene. Prior to this shift, a broad, retro-arc foreland basin stretched across western North America in response to flexural loading by the Sevier fold and thrust belt (DeCelles, 2004). Beginning in Late Cretaceous time, exhumation of basement-cored uplifts (i.e., the "Laramide Orogeny") dissected this contiguous foreland basin (Cather, 2004; Coney & Reynolds, 1977; Dickinson & Snyder, 1978; Gries, 1983), which disrupted and rerouted pre-existing drainage networks, while recycling foreland basin sediments, and exhuming older sources (Dickinson et al., 1988; Lawton, 2008). Many researchers interpret shallow angled subduction of the Farallon slab and the conjugates of the Shatsky and Hess oceanic plateaus

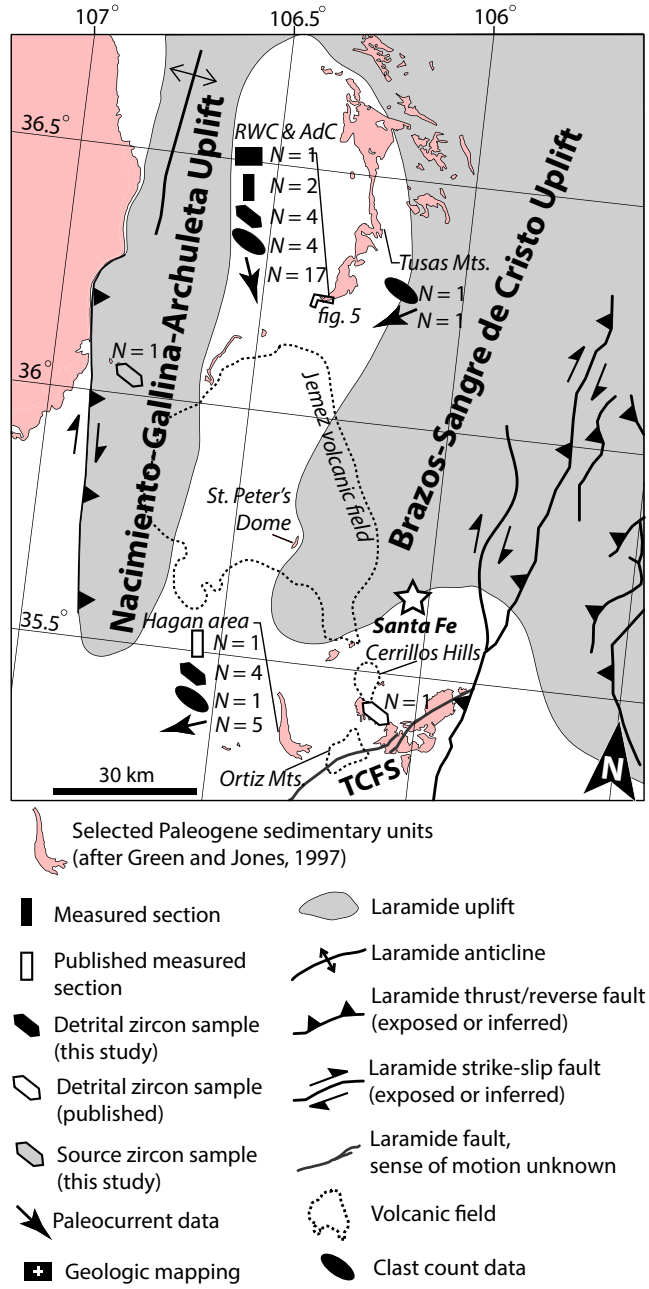

FIGURE 3 Map of north-central New Mexico displaying data type and collection locations, which show the number of each type of dataset for each location (N). The published detrital zircon sample location directly south of the Cerrillos Hills is from the Espinaso Formation (Sharman et al., 2016). Paleocurrent arrows indicate measurement contributed by this study. RWC -Red Wash Canyon, AdC- Arroyo del Cobre, TCFS-Tijeras-Cañoncito fault system. Uplift geometries and faults modified from Cather (2004) and Lisenbee (2013). Selected Paleogene sedimentary rock polygons include the El Rito, Galisteo, Diamond Tail, and San Jose formations (after Green & Jones, 1997)

beneath western North America to have driven the transition from Sevier thin-skinned fold-and-thrust belt deformation to basement-involved, intra-foreland faulting (Coney & Reynolds, 1977; Copeland, Currie, Lawton, & Murphy, 2017; Dickinson & Snyder, 1978; Humphreys, 2009; Liu et al., 2010; Liu & Currie, 2016; Tarduno, McWilliams, Debiche, Sliter, & Blake, 1985). Basement-involved uplifts produced a series of broken foreland and intermontane basins (DeCelles, 2004), which serve as a patchwork record of Late Cretaceous-early Paleogene tectonic activity and drainage dynamics.

2.1.1 | Laramide basin development & deformation in north-central New Mexico

The El Rito, Galisteo, and Diamond Tail formations are interpreted to be deposited within a single Laramide basin (Dickinson et al., 1988; Ingersoll, Cavazza, Baldridge, & Shafiqullah, 1990; Lucas, 1984; Yin & Ingersoll, 1997), one of several north-south trending "axial" basins developed between "perimeter" basins to the east and "ponded" basins to the west (Dickinson et al., 1988). Dickinson et al. (1988) defined axial basins as elongate depocenters with small areas, high-relief margins, and dominated by alluvial deposition. Several accommodation mechanisms have been proposed to explain subsidence of the Galisteo and El Rito depocenters. These include deposition within a synclinal sag in the shared hanging wall between two bivergent thrust systems (Yin & Ingersoll, 1997) and deposition in a pull-apart basin formed by dextral transtension (Cather, 1992).

Uplift and exhumation of bounding basement blocks to the El Rito and Galisteo depocenters commenced in the Late Cretaceous. The uplift to the east (i.e., Brazos-Sangre de Cristo (BSC) Uplift) was a dominant sediment source and Galisteo Basin-bounding feature throughout most of the depocenter's existence while the western uplift (i.e., NGA Uplift) remained comparatively insignificant until the Eocene. East and northeast of the El Rito and Galisteo depocenters, east-vergent thrust faults exhumation of the BSC Uplift (Figure 2c; Baltz, 1965; Lindsey, 1998; Lisenbee, 2013). The Sangre de Cristo portion of the uplift provided sediment to the Vermejo Formation by the early Maastrichtian (Bush, Horton, Murphy, & Stockli, 2016). By late Maastrichtian time, the BSC Uplift was contributing igneous and metamorphic basement detritus to the Raton Basin (Figure 2b) (Baltz, 1965; Pillmore & Flores, 1990). West of the El Rito and Galisteo depocenters, stratigraphic thinning of the upper Campanian (~75 Ma) Pictured Cliffs Sandstone marks initial activation of the Nacimiento Uplift (Figure 2b, Baltz, 1967; Cather, 2004; Woodward, 1987). Apatite fission-track (AFT) ages along the Nacimiento Uplift increase northward, from middle Eocene–earliest Oligocene ages (46 ± 5 to 33 ± 4 Ma) in the south, to Late Cretaceous–middle Eocene ages (81 ± 8 to 46 ± 7 Ma) in the north (Kelley, Chapin, & Corrigan, 1992). Kelley et al. (1992) favor a middle Eocene onset of exhumation and cooling; they attribute the wide range of ages in the north to

less exhumation and exposure of incompletely reset thermochronometers. The Gallina-Archuleta Uplift is interpreted as the northward continuation of the Nacimiento Uplift (Lucas, 1984; Woodward et al., 1992). The Galina-Archuleta Uplift preserves Cretaceous strata at its crest, consistent with the observed northward trend of decreased exhumation observed in the Nacimiento Uplift. Yin and Ingersoll's (1997) model interprets the BSC and NGA uplifts as the east and west edges, respectively, of the bivergent fault system.

The precise timing of cessation of basement-involved shortening in north-central New Mexico is debated (Lisenbee, 2013). North-striking dextral faults that cut the Galisteo Formation are interpreted to indicate that north-northeast shortening-driven deformation lasted at least until latest Eocene (Erslev, 2001; Lisenbee, 2013). Recent mapping of the Espinaso Formation (stratigraphically above the Galisteo Formation) supports even younger basement-involved shortening in New Mexico (earliest Oligocene), and would therefore overlap with an early phase of late Eocene–early Oligocene volcanism (Lisenbee, 2013).

2.1.2 | New Mexico volcanism

The Cretaceous–middle Eocene was marked by brief pulses of volcanism that were most dominant in southern New Mexico and southern Colorado (i.e., the Colorado Mineral Belt) (Chapin, Wilks, & McIntosh, 2004). Cretaceous and Paleocene volcanism was restricted to the southernmost part of New Mexico where magmatic conduits exploited Proterozoic sutures (Chapin et al., 2004; Karlstrom & Bowring, 1988; Karlstrom & Humphreys, 1998). Activity increased and swept northward from early to late Eocene, and has continued to present, with a brief lull during the middle Miocene (Chapin et al., 2004). Prior to the middle Miocene, intermediate and felsic volcanism was dominant, whereas subsequent volcanic activity was predominantly basaltic (Chapin et al., 2004). From late Eocene through Oligocene time (37–23 Ma), New Mexico experienced three periods of explosive ignimbrite volcanism (Chapin et al., 2004). The first of these three eruptive episodes occurred between 37.5 and 31.4 Ma, and therefore overlaps with late-stage, basement-involved shortening. This initial pulse primarily affected the Trans-Pecos and Mogollon-Datil regions in west Texas and southwest New Mexico, respectively (Figure 2), but some volcanic activity stretched into north-central New Mexico (Cather, 1990; Chapin et al., 2004). The role of explosive volcanism is particularly important to sediment character, as distribution of volcanic material over a broad area may have affected drainage networks that would not otherwise contain any upstream volcanic source. Increased volcanic activity resulted in a transition from quartz-rich to volcaniclastic sedimentation between the Galisteo and Espinaso formations (Lisenbee, 2013; Smith et al., 1991; Stearns, 1953), which occurred at ~38 Ma (Prothero & Lucas, 1996).

2.1.3 | Stratigraphy of the El Rito and Diamond Tail-Galisteo depocenters

The El Rito Formation is exposed north of Jemez Caldera (Figures 2 and 3) and is identified by its brick-red color, coarse-grained sandstones, and quartzite clast-dominant, cobble–boulder conglomerate lithology (Bingler, 1968). Heretofore, the thickest documented section of El Rito Formation was ~60 m in the Ortega Mountains (Bingler, 1968), which is part of the Tusas Mountains (Figure 3). The absence of absolute depositional chronology has rendered age assignment for the El Rito Formation difficult, and the unit was assumed to be roughly correlative with the Eocene Galisteo Formation (Baltz, 1978; Cather, 2004; Logsdon, 1981; Lucas & Ingersoll, 1981). However, recently Donahue (2016) assigned a 32.3 ± 3.2 (1σ) Ma depositional age based on detrital zircon U-Pb maximum depositional ages. A high-relief angular unconformity separates the basal conglomerates of the El Rito Formation from the underlying rocks that range from Precambrian to Cretaceous age (Cather, 2004). Exposure of the El Rito Formation is limited, but a fining trend from northeast to southwest is discernable (Logsdon, 1981). Paleocurrent data generally indicate a southerly sediment transport direction (Logsdon, 1981). The El Rito Formation is disconformably overlain by the Oligocene Ritito Formation, but this contact is reported as locally conformable in a few locations (Bingler, 1968).

The Diamond Tail and Galisteo formations are exposed in the Galisteo depocenter (Figure 3, Lucas et al., 1997), which is located ~100 km south of the El Rito depocenter. The Diamond Tail Formation was not recognized as a stratigraphic unit separate from the Galisteo Formation before Lucas et al. (1997), but this stratigraphic interval was noted to thin north-northwestward by >700 m over approximately 15 km (Gorham & Ingersoll, 1979). The Diamond Tail Formation is thickest in the Hagan area (442 m, Figure 3), sits unconformably above the Cretaceous Menefee Formation, and is informally divided into lower, middle, and upper members (Lucas et al., 1997). The lower and upper members of the Diamond Tail Formation comprise predominantly amalgamated, sharp-based sandstones containing rip-up clasts, and fossil logs, whereas the middle member is primarily variegated mudstone (Lucas et al., 1997). The Diamond Tail Formation is assigned to the late Paleocene–early Eocene based on the lowermost Eocene index fossil (*Hyracotherium* sp.) identified in the upper portion of the middle member (Cather, Connell, Lucas, Picha, & Black, 2002; Lucas et al., 1997).

The Diamond Tail Formation is unconformably overlain by the Galisteo Formation, which is 979 m thick in the Hagan area (Lucas et al., 1997). Biostratigraphic data indicates that

the Galisteo Formation spans most of the Eocene (Lucas, 1982; Lucas & Williamson, 1993). However, the same index fossil (*Hyracotherium* sp.) is found in the middle Diamond Tail Formation is also found in the lower Galisteo Formation, indicating that the intra-formational unconformity represents ≤6 M.y. (Cather, 2004; Woodburne & Swisher, 1995). The El Rito and Galisteo formations have been interpreted as coeval deposits that share a proximal to distal relationship, respectively (Baltz, 1978; Cather, 2004; Gorham, 1979; Gorham & Ingersoll, 1979; Logsdon, 1981; Lucas, 1984; Yin & Ingersoll, 1997). The Galisteo Formation records fluvial deposition (Baltz, 1978; Gorham, 1979; Stearns, 1943) and is informally divided into an upper and lower member based on mappable lithofacies relationships (Lisenbee, 2013; Lucas et al., 1997). The BSC and NGA uplifts are invoked as the primary sources of sediment for the Diamond Tail and Galisteo formations (Cather, 1992; Gorham, 1979; Gorham & Ingersoll, 1979; Lucas et al., 1997).

The northernmost exposure of the Galisteo Formation outcrops at St. Peters Dome (Figure 2), which is located approximately midway between the El Rito and Galisteo depocenters. The unit at this location is over 600 m thick and exhibits a generally coarsening upward trend from sand-dominated lithofacies at the base to cobble-dominated lithofacies in the upper section (Cather, 1992). The overall coarser lithofacies and generally southward paleocurrents suggest a proximal to distal relationship between the Galisteo Formation exposed at St. Peters Dome and the more southern locality described above (Cather, 1992).

The Galisteo Formation is in gradational contact with the overlying Espinaso Formation. The formational contact is identified by a transition from quartz- to volcaniclastic-rich sandstone composition (Stearns, 1953). The volcaniclastic sandstones, clast- and matrix-supported conglomerates, and poorly welded pyroclastic deposits of the Espinaso Formation comprise ~430 m of sedimentary rock (Kautz, Ingersoll, Baldridge, Damon, & Shafiqullah, 1981). In the Hagan area (Figure 3), paleocurrent data indicates strong west-directed sediment transport (Cather et al., 2002). The primary sediment source for the Espinaso Formation is attributed to contemporaneous volcanic activity in the Ortiz Mountains and Cerrillos Hills (Figure 3), ~10 km east and ~20 km northeast, respectively (Kautz et al., 1981). Deposition of the Espinaso Formation spans from ~38 Ma (Prothero & Lucas, 1996) to ~30 Ma (Kay, 1986; Lisenbee, 2013).

2.1.4 | The Laramide province & the Gulf of Mexico

Withdrawal of the Western Interior Seaway in the late Cretaceous opened a fluvial corridor that connected North America's western interior to the western margin of the Gulf of Mexico (Blum et al., 2017). Fluvial pathways and discharge into the gulf were controlled by several long-lived structural embayments whose up-dip catchments expanded and contracted in response to tectonic forcing (Blum et al., 2017; Galloway et al., 2011). During the Paleogene, sediment supply was predominantly controlled by tectonic activity and inactivity within the Laramide province (Galloway, 2002). Western interior-derived sediment was delivered to the Gulf of Mexico by a few transcontinental river systems (Galloway et al., 2011). Different interpretations propose that the El Rito and Galisteo depocenters drained into either the paleo-Colorado-Brazos River (Blum et al., 2017), or into paleo-Colorado and Rio Grande rivers (Galloway et al., 2011) throughout Paleocene–Eocene time.

Although previously discriminated as two separate systems, recent paleogeographic reconstructions suggest that the paleo-Colorado and Houston-Brazos fluvial-deltaic systems were, if not identical, at least geographically and temporally overlapping. These two fluvio-deltaic systems were distinguished as two separate sediment sources to the Gulf of Mexico based on sandstone petrography (Galloway et al., 2011; Loucks, Dodge, & Galloway, 1986). However, Blum et al. (2017) combined the Colorado and Houston-Brazos systems into the paleo-Colorado-Brazos fluvial network based on detrital zircon U-Pb data. In the fluvial model of Galloway et al. (2011) portions of the Colorado and Houston-Brazos rivers' inputs occupy similar geographic areas in interleaved stratigraphic intervals throughout the Paleocene–Eocene. Their model also proposes that the Colorado River disappeared as a major fluvial input during the mid-Eocene because its catchment was captured and divided between the paleo Rio Grande and Houston-Brazos River (Galloway et al., 2011). During that time, the Houston-Brazos fluvio-deltaic system resided on top of the older paleo-Colorado River delta (Galloway et al., 2011). In light of these numerous overlaps, we consider the paleo Colorado and Houston-Brazos fluvial systems to be a dynamic continuum of drainage primarily sourced by the expanding and contracting central and southern Laramide province catchment sensu Blum et al. (2017) and use the Colorado-Brazos terminology.

2.2 | Potential Paleogene sediment sources

We define twelve sediment sources that were potential contributors of detritus to the El Rito and Galisteo depocenters (Table 1). We also describe two conditional sources that are applied sparingly in mixture modeling of basin samples (see *DZmix* description below), but provide important insight where applicable. Below we describe potential sources from oldest to youngest, and include location, lithology, and detrital zircon U-Pb age distributions (see Table 1 for references).

The oldest sources include metamorphic and igneous basement: the ~1.7 Ga Ortega Quartzite (similar depositional age and detrital zircon unimodal age distribution; Jones,

TABLE 1 Summary of source group zircon geochronologic data used in this paper, both generated in this study and collected from previous publications

Source profile	Source group	Rock type	Unit(s)	PDP figure	*N*	*n*	References
Source profile 1	Magmatic arc	Sandstone	Kaiparowits and Uinta fms.	Figure 4a	3	282	Lawton and Bradford (2011), Dyman et al. (2008), Laskowski et al. (2013)
	Late Cretaceous	Sandstone	Mancos Shale and Mesa Verde Gp.	Figure 4b	7	683	Dickinson and Gehrels (2008b)
	Early Cretaceous	Sandstone	Dakota Fm.	Figure 4c	2	228	Bush et al. (2016)
	Jurassic	Sandstone	Morrison Fm.	Figure 4d	4	363	Dickinson and Gehrels (2008b)
	Triassic	Sandstone	Chinle Fm.	Figure 4e	2	168	Dickinson and Gehrels (2008a)
	Eolianites	Sandstone	Entrada, Navajo, and Wingate fms.	Figure 4f	5	468	Dickinson and Gehrels, (2003)
	Late Paleozoic (NE)	Sandstone	Sangre de Cristo Fm.	Figure 4g	1	155	this study
	Late Paleozoic (NW)	Sandstone	Madera Formation and Cutler Gp.	Figure 4h	2	280	this study
	Cambrian gr.	Granite	Florida Mountain Gr.	Figure 4i	1	15	Amato and Mack (2012)
	Picuris Orogenic gr.	Granite	Caballo Mountain Gr.	Figure 4j	1	15	Amato and Becker (2012)
	Ortega Quartzite	Quartzite	Ortega Quartzite	Figure 4k	2	226	Jones et al. (2009, 2011)
	Nacimiento gr.	Metagranite	Precambrian (undivided)	Figure 4l	1	22	this study
SJ	San Jose Fm.	Sandstone	San Jose Formation	Figure 4m	2	181	Donahue (2016)
App	Appalachian	Sandstone	Greene, Washington, Pottsville, Bluestone, Hinton, and Price fms.	Figure 4n	5	515	Becker, Thomas, Samson, and Gehrels (2005), Becker, Thomas, and Gehrels (2006), Park, Barbeau Jr., Rickenbaker, Bachmann-Krug, and Gehrels (2010)

Abbreviations: Fm., formation; fms., formations; Gp., Group; gr., granite/granitoid; NE, northeast, NW, northwest. Further detail is provided in Appendix 4.

Connelly, Karlstrom, Williams, & Doe, 2009) (Figure 4k), the ~1.7 Ga Nacimiento granitoid (Figure 4l), the ~1.4 Ga Picuris Orogeny granitoid (Daniel et al., 2013) (Figure 4j), and ~500 Ma Cambrian igneous rocks (Figure 4i), each of which have roughly unimodal zircon age distributions of their respective ages. The Ortega Quartzite outcrops in the Tusas Mountains, which border the northeast edge of the study area (Figure 3). Its absence in the NGA Uplift makes the Ortega Quartzite an important source indicator of the BSC Uplift in local north-central New Mexico basins. Igneous and meta-igneous rocks of the Yavapai-Mazatzal terrane including the Nacimiento granitoid outcrop are exposed in the NGA Uplift to the west, BSC Uplift to the east and north, and Montosa Uplift to the south (Figure 2c). Picuris Orogenic granitoids (Figure 4j) are exposed primarily in the NGA and northern Montosa uplifts. Cambrian igneous rocks have limited surface exposure, but are found in the Lobo and Pedernal Hills and Florida Mountains in New Mexico (Figure 2c), and in the Wet Mountains of central Colorado (Loring & Armstrong, 1980; McMillan & McLemore, 2001; Schoene & Bowring, 2006).

Paleozoic sedimentary sources include Pennsylvanian-Permian rocks to the east and west of the El Rito and Galisteo depocenters (Figure 4g and H, respectively). The presence of these sources indicates recycling of sedimentary rocks from the Paradox and Taos basins, and may suggest broader source areas than just the NGA and BSC uplifts. Northwestern Pennsylvanian–Permian rocks exhibit a predominantly unimodal detrital age distribution of ~1.7 Ga (Figure 4h), whereas coeval rocks to the northeast exhibit a bimodal detrital age distribution with populations centered around ~1.4 and ~1.7 Ga (Figure 4g).

The recycled Appalachian foreland basin source (Figure 4n) is one of two conditional source groups and is comprised of detrital zircon spectra from late Mississippian to Permian sedimentary rocks in the Appalachian Basin (Figure 4n, Table 1). This is considered a conditional source group because sediment directly sourced from Appalachian Basin rocks could only be recycled to the Gulf of Mexico and could not be a source for Laramide basins during the Paleogene (Galloway et al., 2011). Appalachian Basin deposits exhibit

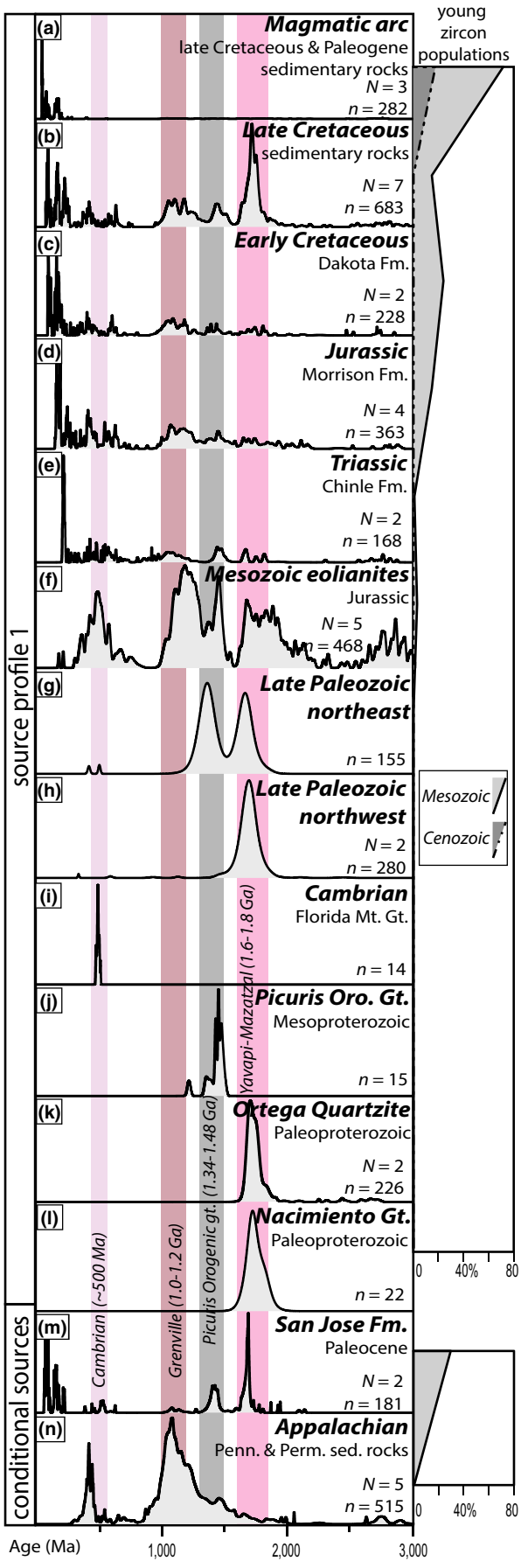

FIGURE 4 Detrital zircon data for source groups showing the primary source profile (a–l) and conditional sources (m and n). Each probability density plot (PDP) corresponds to a source group discussed in the text and indicated by the bold and italicized name in the top right corner of the respective PDPs. The San Jose Formation and Appalachian composite sources are added to source profile 1 to make conditional source profiles 1_SJ, 1_App, and 1_SJ+App. See Table 1 for sample references and Appendix 4 for further sample metadata details. Vertical color swatches on PDPs indicate common reference detrital populations. Age range of reference populations Yavapai-Mazatzal, Picuris Orogenic granitoid, and Grenville are from Laskowski et al. (2013). The young zircon population column displays the percentage of Mesozoic and Cenozoic age zircons in the respective source group described on the PDP to the left. Source group PDP metadata is available in Table 1. Gt., granitoid; Mt., mountain; Oro., orogenic; Penn., Pennsylvanian; Perm., Permian; sed., sedimentary

a multimodal distribution containing significant populations at 1.3–1.0 Ga, and ~450 Ma, and subordinate populations at 3.0–2.5 Ga and 2.0–1.6 Ga.

Lower Mesozoic sedimentary sources include Jurassic eolianites (Navajo, Wingate, and Entrada formations) (Figure 4f), which are widely distributed across the four corners area (Utah, Colorado, New Mexico, and Arizona) of western North America (Dickinson & Gehrels, 2003). Abundant basement-derived detritus was shed from the northern and western flanks of the BSC Uplift since the Late Cretaceous (Bush et al., 2016) and latest Paleocene-earliest Eocene (Cather, 2004; Smith, 1992), respectively, indicating that the BSC had been largely stripped of Mesozoic sedimentary cover. Therefore, within north-central New Mexico, the presence of recycled Mesozoic sedimentary strata in middle Eocene and younger basin fill is consistent with derivation from NGA Uplift. Eolian deposits exhibit a complex, multimodal distribution with significant populations at 3.0–2.5, 2.0–1.6, 1.3–1.0 Ga, and ~500 Ma (Figure 4f). Jurassic eolianites also exhibit multiple age modes spanning from 330 to 800 Ma with minor contributions between 300 and 180 Ma. The next two potential sources are the Triassic Chinle Formation (Figure 4e) and the Jurassic Morrison Formation (Figure 4d). Both formations outcrop across northern New Mexico and exhibit similar multimodal detrital zircon age distributions with notable age peaks of similar proportion at ~1.7 and ~1.4 Ga, a 1.3–1.0 Ga (Grenville) population, and an irregular distribution of Paleozoic and younger ages with dominant subpopulations in the Mesozoic.

Cretaceous rocks compose the next two potential sediment sources, and include the Lower Cretaceous fluvial sandstones of the Dakota Formation (Figure 4c), and Upper Cretaceous siliciclastic rocks (i.e., Mesa Verde Group and Mancos Shale) (Figure 4b), which are exposed across northern New Mexico. Cretaceous formations show similar

detrital zircon age distributions with populations of ~1.5 Ga, 1.3–1.0 Ga, 700 Ma, 400 Ma, and increasing abundances of 250–100 Ma ages skewed toward younger ages. The notable exception is the presence of a dominant ~1.8 age mode in Upper Cretaceous strata that is nearly absent in the early Cretaceous (Figure 3b–c).

The source containing the youngest zircons is the magmatic arc group (Figure 4a), comprised of samples of Upper Cretaceous and Paleogene strata from southern Utah (Laskowski, Decelles, & Gehrels, 2013). The magmatic arc source contains a notable peak at ~48 Ma, and populations at 70–110 and 140–180 Ma.

The Paleocene San Jose Formation is the second conditional source group (Figure 4m) and is comprised of two detrital zircon samples from the San Jose Formation of the San Juan Basin (Donahue, 2016).We characterize it as a conditional source group because it is interpreted to be deposited by earliest Eocene fluvial system that flowed through the Galisteo depocenter area on its way to the Gulf of Mexico (Galloway et al., 2011), and is therefore temporally and spatially limited in its application.

TABLE 2 Description of lithofacies used to describe measured sections

Lithofacies	Description
Mm	Mudstone, massive/structureless
Ml	Mudstone, laminated
Mr	Mudstone, rippled
Mh	Mudstone, horizontal bedded
Sl	Sand, laminated
Sr	Sand, rippled
Sh	Sand, horizontal bedded
Sp	Sand, planar cross-bedded
St	Sand, trough cross-bedded
Sf	Sand, foresets (unable to distinguish type)
Sx	Sand, soft-sedimentary deformation
Sm	Sand, massive/structureless
Gci	Gravel, clast-supported, imbricated
Gct	Gravel, clast-supported, trough cross bedded
Gch	Gravel, clast-supported, horizontal bedded
Gcm	Gravel, clast-supported, massive/structureless
Gmm	Gravel, matrix-supported, massive/structureless

Source: Adapted from Miall (1978).

3 | METHODS

We employ a suite of tectono-stratigraphic tools and previously published data including geologic maps, stratigraphic sections, lithofacies and paleocurrent analyses, conglomerate clast-counts, and detrital zircon U-Pb geochronology to investigate deformation, basin development, and drainage reorganization recorded in the El Rito and Galisteo depocenters.

3.1 | Stratigraphic Analysis

Sections were measured using a standard 1.5 m Jacob's staff, and logged using lithofacies codes adapted from Miall (1978) (Table 2). Bedding geometry, lithofacies associations (Table 3), and auxiliary sedimentary features are also included in stratigraphic descriptions. In Red Wash Canyon and Arroyo del Cobre (Figure 5) the El Rito Formation was measured at decimeter resolution. The surrounding area was mapped to determine facies distributions and stratigraphic relationships (Figures 5 and 6). In the Galisteo depocenter samples were collected in the context of existing stratigraphic sections that cover the Diamond Tail and Galisteo formations (Gorham & Ingersoll, 1979; Lucas et al., 1997), which we augmented with our field observations (Figure 7).

3.2 | Paleocurrent analysis and clast counts

Paleocurrent measurements were taken from trough cross-stratified sandstones, clast-supported, imbricated conglomerates, and (rare) primary current lineations. Trough cross-stratification measurements follow methods outlined by DeCelles, Langford, and Schwartz (1983). All measurements were tilt corrected using S*tereonet 9* (Cardozo & Allmendinger, 2013).

Clast counts were collected ($n \geq 100$) in conglomeratic units and were counted on an approximately 100 × 100 cm grid. Clasts were divided into seven different categories based on lithology: quartzite, vein quartz, chert, conglomerate, sand/mudstone, meta-rhyolite, and granite.

3.3 | Detrital Zircon U-Pb geochronology

Approximately 2 kg of each detrital zircon sample were crushed, and disc milled to ≤400 μm disc spacing. Zircons from each sample were separated using standard separation techniques: hydraulic separation through a water table, density separation using methylene iodide (3.28 g/cm^3), and magnetic separation on a Frantz Isodynamic Magnetic Separator. Grains were washed in nitric acid before being non-discriminately hand-picked under an Olympus SZX12 microscope and mounted on double-sided tape.

Zircon U-Pb age dates were determined at the University of Houston via laser-ablation inductively-coupled-plasma mass-spectrometry using a Photon Machines Analyte 193 ArF excimer laser attached to a pulse counting detector fitted to a Varian 810 quadrupole mass spectrometer (Shaulis, Lapen, & Toms, 2010). Analyses were

TABLE 3 Description of characteristics used to define facies associations

Code	Facies association	Description
GDB	Gravel-dominated braided stream	Identified by the dominant presence of clast-supported conglomerates (Gci, Gct, Gch and Gcm). Erosive basal surfaces. Commonly associated with channel-shaped lenses of medium to very coarse St and Sm containing gravel floaters and lenses
SDB	Sand-dominated braided stream	Identified by the dominant presence of amalgamated medium to very coarse-grained sandstone bodies. St is the most common lithofacies and sandstones often contains gravel floaters and lenses. Fining upward profiles are abundant. Two characteristics are used to distinguish **SDB** from **MB**: (a) lack of laterally accreting surfaces, and (b) infrequent association with **FP** lithofacies association
MB	Sand-dominated meandering stream	Identified by the dominant presence of amalgamated medium to very coarse-grained sandstone bodies that commonly fine upwards. **FP** elements are commonly interbedded with multi-story sandstone bodies. St and Sr are the most common lithofacies and sandstones often contain floating gravel clasts, but more frequently contain intrabasinal clasts (i.e., rip-ups). Two characteristics are used to distinguish **MB** from **SDB**: (a) notable presence of laterally accreting surfaces, and (b) ubiquitous association with **FP** lithofacies association
FP	Flood plain	Identified by the heterogenous assemblage of flood plain elements: flood plain, crevasse splays, and levee complexes. Flood plain deposited sediments are commonly structureless (Sm or Mm) due to pedogenic processes. Pedogenic fabrics such as caliche, rhizoliths, reduced root haloes, blocky ped fracture, and pedogenic slickensides are abundant. Terrestrial burrows are also common. Crevasse splays are identified by tabular sandstones interbedded with mudstones. Internally they are commonly structureless, but also may exhibit normal grading and Sr (sometimes climbing ripples). Levee complexes are identified as coarsening upward successions of sandstone beds (lenticular and tabular [at outcrop scale]) Commonly Sm and Sr, and are often associated with flood plain mudstones.
SGF	Unconfined sed. gravity flow	This uncommon lithofacies association is identified by its medium to very coarse massive/structureless sandstone. Abundant floating gravel clasts. Occasional gravel stringers suggest minor episodes of stream activity.
M	Marine	This rare lithofacies association is identified by the presence of marine fossils and glauconite within siliciclastic mudstone to sandstone.
V	Volcanic	This rare lithofacies association is identified by the presence of volcanic tuff

performed using a 25–30 μm spot size and 240 shots at 10 Hz repetition rate, resulting in approximately 24 s of ablation with 7 s of background measurement followed by 13 s of washout.

Analysis involved repeat measurements of a primary standard after every 10 unknowns. The primary standard used to correct for inter- and intra-element fractionation (Gehrels, Valencia, & Ruiz, 2008) was zircon from a Bohemian Massif potassic granulite *Plešovice* with an ID-TIMS age of 337.13 ± 0.37 (2σ) Ma (Sláma et al., 2008). The uncertainty resulting from this correction is typically 1%–2% (2σ) for both $^{206}Pb/^{207}Pb$ and $^{206}Pb/^{238}U$ ages. To ensure machine stability and to provide a comparison for the primary standard, an external zircon standard was used from the Duluth Complex (*FC5z*) with an accepted age of 1,099.1 ± 0.5 (2σ) Ma, similar to that of AS3 and FC1 from Paces and Miller (1993).

Ages were calculated using *UPbToolbox*, a MATLAB-based graphical user interface that calculates integrated isotopic ratios from raw counts per second measurements exported from Quantum software, corrects for machine bias and fractionation, and filters the data based on user-defined parameters (Sundell, 2017). The best-age transition for younger $^{206}Pb/^{238}U$ ages and older $^{207}Pb/^{206}Pb$ was set to 1,250 Ma. The final data table includes analyses that are between −5% and 20% discordant based on $^{206}Pb/^{238}U$ and $^{207}Pb/^{235}U$, and uncertainties of <15% for ages >600 Ma. In lieu of a common Pb correction (Stacey & Kramers, 1975) for ages <600 Ma, we accept grains whose 2σ uncertainty envelope is <15% discordant by comparison of the $^{206}Pb/^{238}U$ and $^{207}Pb/^{235}U$ ages. UPbToolbox was also used to produce all probability density plots (PDPs) of detrital zircon U-Pb data for detrital source groups and Paleogene sedimentary rocks (see Appendix 3 for raw and reduced data tables). Metadata for Laramide sink samples are presented in Table 4.

3.3.1 | Maximum depositional age

Detrital zircon geochronology can be used to establish the maximum depositional age (MDA) of sedimentary rocks (Dickinson & Geherls, 2009). This method produces MDAs closest to the depositional age of the rocks when there is proximal and contemporaneous volcanism within the catchment (Coutts, Matthew, & Hubbard, 2019; Hilbert-Wolf et al., 2017).

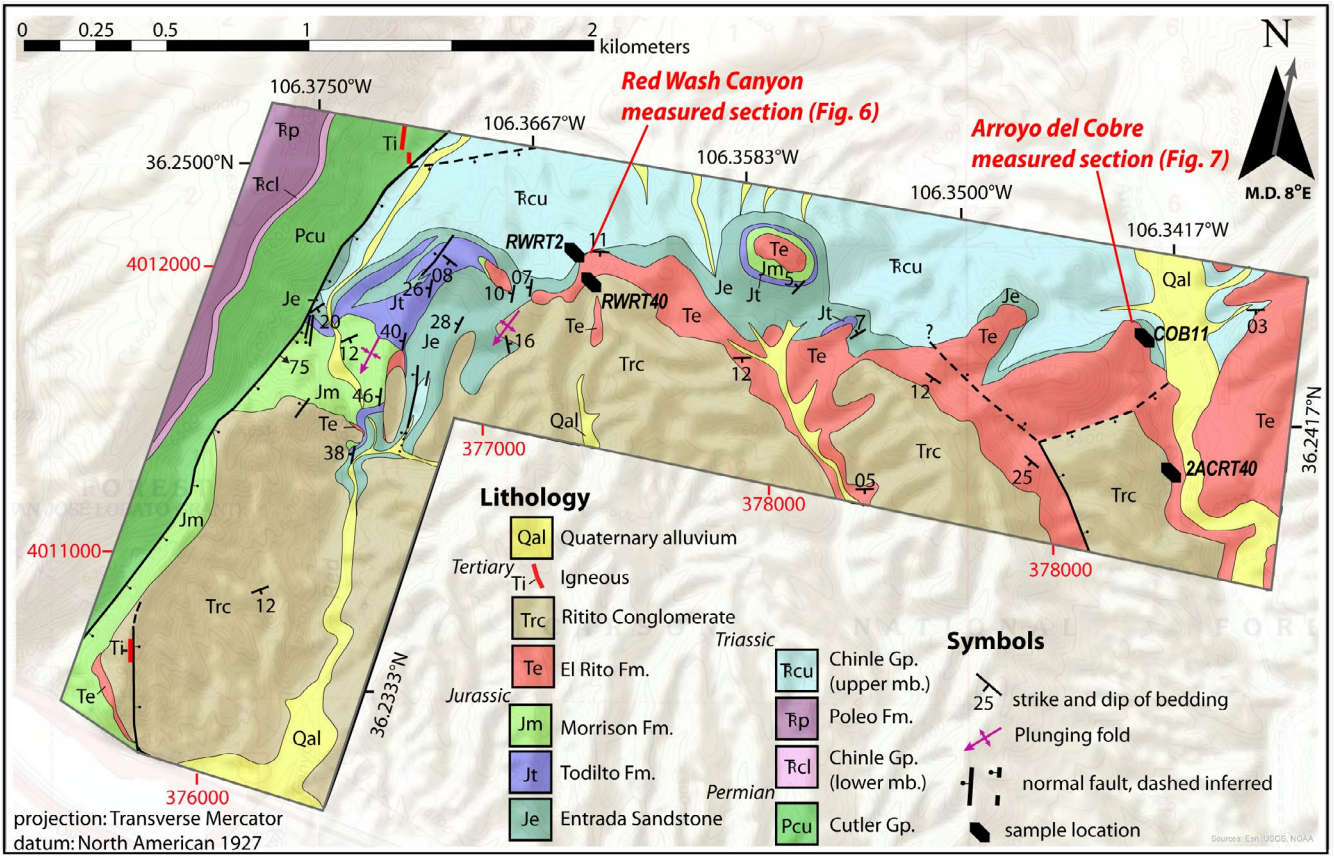

FIGURE 5 Geologic map of Red Wash Canyon and Arroyo del Cobre region, New Mexico highlights the high-relief basal unconformity and the westward thinning of the El Rito Formation. The map combines mapping observations made in this study and modifications of geologic maps from Kelley et al. (2005) and Maldonado (2008)

We used four methods to determine MDA for the three samples containing ample groups of Cenozoic–age zircons (Figure 8, Table 5). (a) The absolute youngest age possible is the youngest single grain (YSG, Dickinson & Gehrels, 2009). (b) The weighted mean of the three youngest grains (WM), can provide a more statistically robust approach but lacks a robust cut-off criterion for older ages (Dickinson & Gehrels, 2009; Hilbert-Wolf et al., 2017). (c) Youngest 1σ grain cluster (YC1σ) calculates MDA by identifying the youngest cluster of grains with overlapping 1σ uncertainty ($n \geq 2$) and determining their weighted mean (Dickinson & Gehrels, 2009). (d) Youngest 2σ grain cluster (YC2σ) is similar to YC1σ, but uses the youngest cluster of grains overlapping at 2σ uncertainty ($n \geq 3$) to calculate the weighted mean (Dickinson & Gehrels, 2009).

3.3.2 | Detrital zircon mixing model

We use the detrital zircon mixing model, *DZmix* (Sundell & Saylor, 2017), to aid in provenance interpretation of U-Pb geochronologic data. This MATLAB-based detrital zircon mixing model uses an inverse Monte Carlo approach to determine the proportions of various sources that can account for the age distribution in a derivative, mixed sample. Specifically, the model determines a range of source contributions by scaling each source age distribution by a random set of percent contributions that sum to 100%. This produces a single model age distribution that is quantitatively compared (see below) to a single basin sample. This process is repeated 100,000 times, comparing each randomly generated source mixture model to the same basin sample. The top 100 (0.1%) of all models ranked by Kuiper V (Kuiper, 1960) value are retained to calculate the mean and standard deviation of modeled source contributions. In this model, all potential sediment sources are considered equally likely because it is impossible to know a priori what sediment sources were contributing to the basin at the time of deposition. Setting such priors would effectively make the mixture modeling circular.

We use Kuiper V statistic provided by *DZmix* as the basis for sample-model comparison for the following reasons: (a) it is a well-established statistical method (Kuiper, 1960; Stephens, 1970; Press, 2007), (b) it is equally sensitive across all age ranges (Kuiper, 1960; Press, 2007; Wissink et al., 2018), and (c) our source group data is collected from multiple sources with varying methods of reporting uncertainty, and use of the Kuiper V value does not incorporate uncertainty into the comparisons.

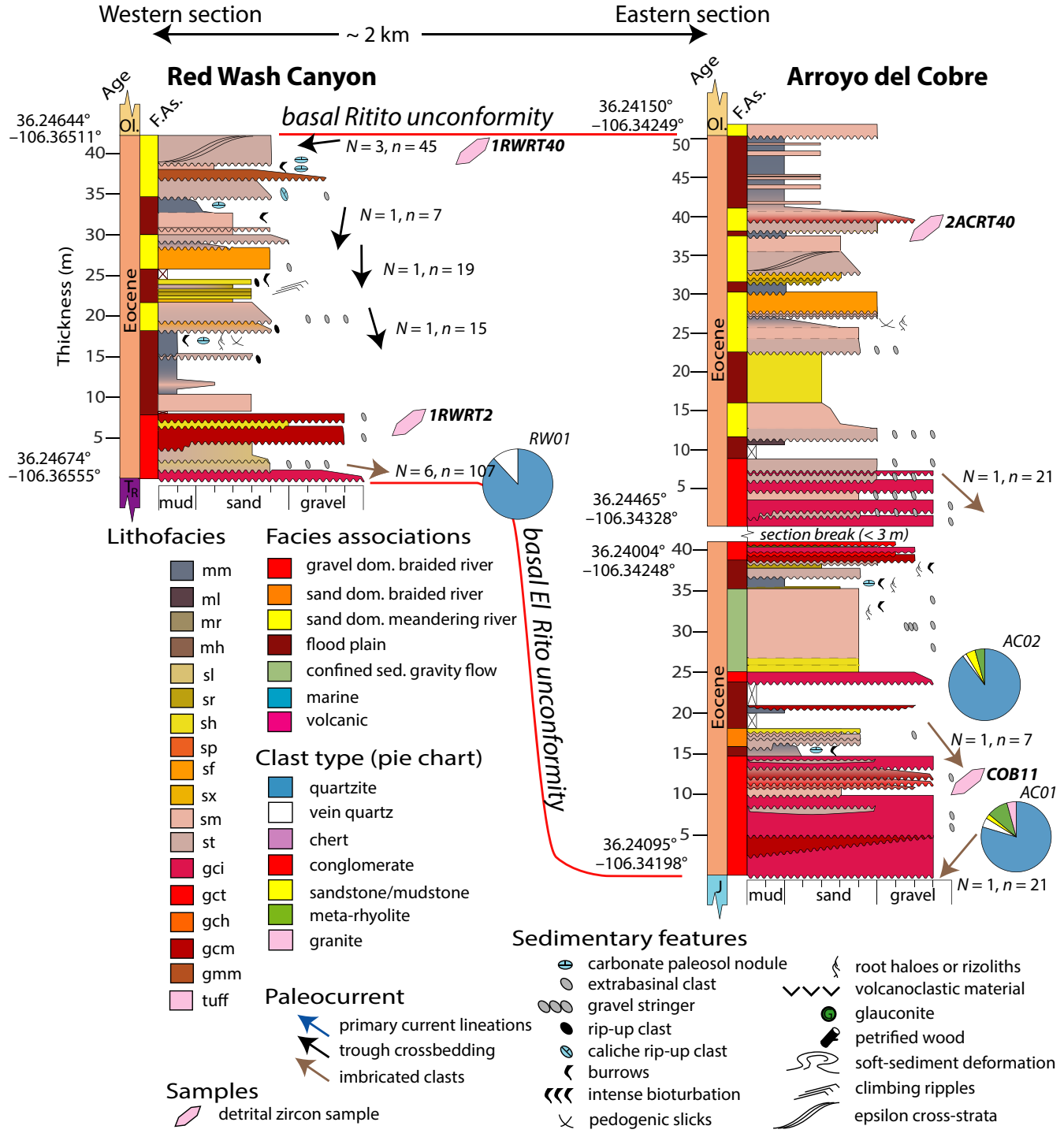

FIGURE 6 Western and eastern measured sections of the El Rito Formation from Red Wash Canyon and Arroyo del Cobre, respectively. See Lithofacies descriptions in Table 2 and lithofacies associations in Table 3. Measured sections show paleocurrent orientations, clast counts, and detrital zircon sample locations. Paleocurrent data and clast count details are provided in supplementary material (Appendices 1 and 2, respectively). *N*- and *n*-values correspond to paleocurrent stations and individual measurements at each station, respectively. F.As, lithofacies association; J, Jurassic; Ol., Oligocene; TR, Triassic

4 | RESULTS

4.1 | Stratigraphy

The El Rito Formation in the Red Wash Canyon (i.e., western) and Arroyo del Cobre (i.e., eastern) areas sits in angular unconformity above Mesozoic stratigraphy and is truncated by a disconformity below the Ritito Formation. The thickest section of the El Rito Formation (1ACRT and 2ACRT, total 92 m) to the east thins westward (RWRT, 41m) inside the erosional relief of the basal unconformity

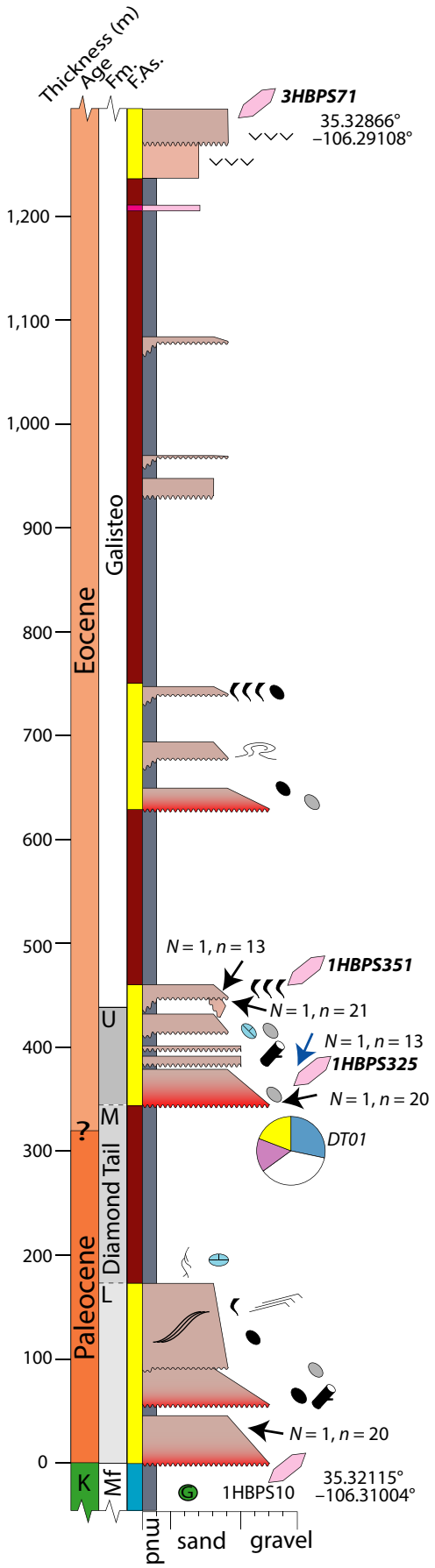

FIGURE 7 Galisteo depocenter measured section showing paleocurrent measurements, clast counts, sample locations, and sedimentary structures. Facies, lithofacies, sedimentary structures, colors, paleocurrent data, clast count, and sample data symbols and description convention follow Figure 6. The section is modified from Gorham and Ingersoll (1979) and Lucas et al. (1997), based on our field observations. F.A.s, facies associations; Fm., formation; K, Cretaceous; L, lower; M, middle; Mf, Menefee Formation; U, upper

(Figure 6). Farther west, thinner deposits of the El Rito Formation only preserve basal conglomerates inside of local erosional lows (channels) while in many other locations the formation is completely removed by the Ritito basal unconformity (Figure 5).

Lithofacies in the bottom half of the eastern section (Arroyo del Cobre) exhibit predominately imbricated, trough cross-stratified or massive cobble–boulder clast-supported conglomerates, which are interbedded with up to meter-thick trough cross-stratified sandstones and pedogenically-altered mudstones. The upper ~40 m preserves finer-grained lithofacies interspersed with erosive, channel-shaped sandstone bodies (commonly >1 m thick) featuring occasional epsilon cross-stratification. Fine–very fine grain sandstones in the upper ~10 m of the El Rito Formation were deposited in tabular (<0.5 m thick), sharp-based, internally structureless beds, and are interbedded with pedogenically-altered mudstones.

The western area (Red Wash Canyon) clearly exposes the onlapping relationship of the El Rito Formation with its high-relief basal unconformity (Figure 9c). The basal 8 meters of El Rito Formation in the western area exhibits similar gravel-dominated lithofacies as the lower ~45 m of the eastern section. An upsection increase in moderate- to well-developed paleosols, bioturbation (Figure 9b), and tabular sandstones indicate a transition to lower energy deposition. At the top of the section (Figure 6) a multi-story, erosive-based sandstone unit exhibits epsilon cross strata and contains basal conglomeratic lags comprised of caliche clasts. The poorly exposed El Rito Formation-Ritito Formation unconformity marks the top of the western measured section.

The Diamond Tail Formation comprises upper and lower members that exhibit sandstone-dominant lithofacies and a middle member that is dominated by muddy, varicolored paleosols (Figure 7) (Lucas et al., 1997). The erosional contact between the Menefee Formation of the Mesaverde Group and the lower member of the Diamond Tail Formation marks the base of the Cenozoic section. The lower member contains thick (5–8 m), multi-story, gravel-based, erosive sandstone units that fine upward and commonly feature trough cross-strata, occasionally nested within meter-scale epsilon cross-strata. Soft sediment deformation is common. Sandstones contain coaly plant fragments and abundant rip-up clasts.

TABLE 4 Summary of Laramide basin detrital zircon geochronologic data used in this paper, both generated in this study and collected from previous publications

Depocenter	Sample	Sample location	Unit	PDP figure	*n*	Latitude	Longitude	References
El Rito	RWRT40	Red Wash Canyon	upper El Rito Fm.	Figure 11a	120	36.24644	−106.36511	This study
	RWRT2	Red Wash Canyon	lower El Rito Fm.	Figure 11b	176	36.24674	−106.36555	This study
	2ACRT40	Arroyo del Cobre	upper El Rito Fm.	Figure 11c	121	36.24004	−106.34248	This study
	COB11	Arroyo del Cobre	lower El Rito Fm.	Figure 11d	110	36.24396	−106.34308	This study
Galisteo	GB001	Galisteo area	Espinaso Fm.	Figure 11e	99	35.42415	−106.06726	Sharman et al. (2016)
	3HBPS71	Hagan area	upper Galisteo Fm.	Figure 11f	119	35.32866	−106.29108	This study
	1HBPS351	Hagan area	lower Galisteo Fm.	Figure 11g	146	35.32446	−106.30341	This study
	1HBPS325	Hagan area	Diamond Tail Fm., upper mb.	Figure 11h	148	35.32405	−106.30358	This study
	1HBPS10	Hagan area	Diamond Tail Fm., lower mb.	Figure 11i	146	35.32115	−106.31004	This study

Note: All sample were collected in north-central New Mexico.
Abbreviations: Fig., figure; Fm., Formation; mb, member. Further detail for newly presented data is provided in Appendix 3.

The middle member of the Diamond Tail Formation is lithostratigraphically identified as a ~150 m variegated mudstone interval (Lucas et al., 1997) and is poorly exposed in the study area. Outcrops are composed of highly weathered badlands featuring bedding-parallel bands of maroon-brown and light grey mudstones (Figure 9d).

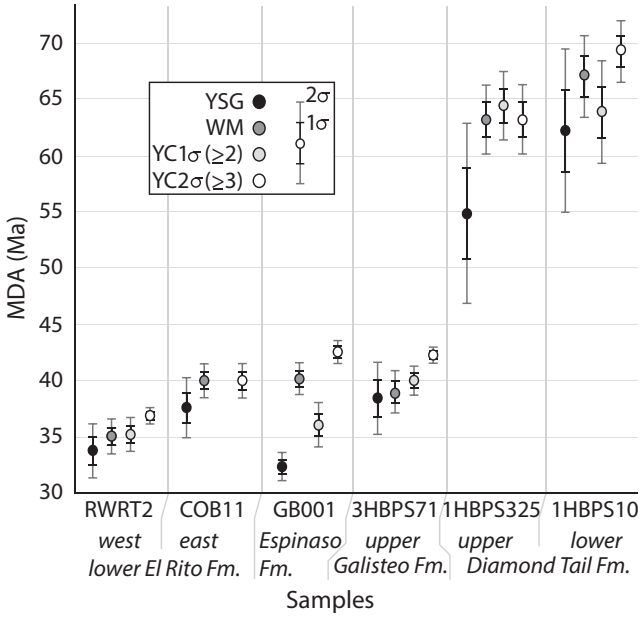

FIGURE 8 Graph of maximum depositional ages (MDAs) for the samples that contained approximately depositional age grains based on gross stratigraphic age control. Sample GB001 is from Sharman et al. (2016). Sample COB11 contains too few depositional age zircons with overlapping 1σ uncertainties to determine a useful YC1σ (≥2) age. WM-weighted mean of three youngest grains, YC1σ (≥2)- youngest cluster of ≥2 grains with overlapping 1σ uncertainty, YC2σ (≥3)- youngest cluster of ≥3 grains with overlapping 2σ uncertainty

The upper member of the Diamond Tail Formation exhibits similar, though slightly coarser facies than the lower member. The top of the upper member is marked by an unconformable contact with the Galisteo Formation. This contact exhibits a regional, but subtle angular unconformity (Cather, 2004). However, the contact also features high-angle (>10° dip) discordance between local rotated blocks of sandstone in the Diamond Tail Formation and the low angle dip of the overlying Galisteo Formation (Figure 9e).

The unconformity at the base of the first sandstone unit of the Galisteo Formation is a mappable feature (Figure 9d). The lower portion of the Galisteo Formation is dominantly mudstone (Gorham & Ingersoll, 1979) and is poorly exposed in the southern Galisteo depocenter. Sandstones of the lower Galisteo Formation are generally finer grained than sandstones found in the Diamond Tail Formation.

The uppermost exposure of the Galisteo Formation is comprised of poorly exposed tuff and intercalated massive volcaniclastic sandstone and mudstone beds. The top of the 3HBPS section is in the upper Galisteo Formation and is characterized by coarse-medium grained trough cross-bedded sandstone bodies (Figure 7) containing abundant volcanic lithic grains. The higher proportion of volcanic lithic grains and the presence of a minor tuff bed indicate proximity to the top of the Galisteo Formation (Lisenbee, 2013; Stearns, 1953), and is the location of detrital zircon sample 3HBPS71.

4.2 | Paleocurrent data

Paleocurrent measurements from the El Rito Formation indicate an upsection rotation from eastward to south and even westward paleoflow in the western (Red Wash Canyon)

TABLE 5 Maximum depositional age determinations (Ma) for the basal El Rito, upper Galisteo, and Espinaso formations. The Espinaso Formation sample contained an insufficient amount of approximately depositional age (criteria described in text) detrital zircons to calculate WM, YC1σ, and YC2σ

Sample	YSG	1σ	WM	1σ	YC1σ (≥2)	1σ	YC2σ (≥3)	1σ
RWRT2	33.8	±1.2	35.1	±0.8	35.3	±0.7	36.9	±0.4
COB11	37.6	±1.3	40.0	±0.7	*no useful population*		40.0	±0.7
GB001	32.4	±0.6	40.2	±0.7	36.1	±1.0	42.6	±0.5
3HBPS71	38.4	±1.6	39.0	±0.9	40.0	±0.6	42.4	±0.4
1HBPS325	54.9	±4.0	63.2	±1.4	64.5	±1.5	63.2	±1.4
1HBPS10	62.3	±3.6	67.0	±1.8	63.8	±2.3	69.2	±1.4

Abbreviations: WM, weighted mean of three youngest grains; YC1σ (≥2), youngest cluster of ≥2 grains with overlapping 1σ uncertainty; YC2σ (≥3), youngest cluster of ≥3 grains with overlapping 2σ uncertainty; YSG, youngest single zircon.

location, but are more consistently southward in the Arroyo del Cobre area, which is 2 km to the east (Figure 10b). Paleocurrent indicators from clast-supported conglomerates in the basal El Rito Formation along the western portion of our study area ($N = 8$, $n = 139$, where N is the number of paleocurrent stations and n is the number of measurements), suggest a consistent east-directed paleoflow (Figure 10b). However, paleocurrent measurements from trough cross beds upsection ($N = 6$, $n = 86$) change and indicate variable south-, and west-directed paleoflow. In contrast, in paleocurrent measurements in the eastern area yield consistently southwest and southeast paleoflow direction ($N = 3$, $n = 49$). Although the El Rito Formation paleocurrent measurements presented herein are in general agreement with an overall southwest paleoflow direction, these data provide higher temporal and spatial resolution than previously reported (Logsdon, 1981).

Imbricated conglomerate clast orientations indicate a southwest paleoflow direction ($N = 1$, $n = 17$) in the alluvial fan facies of the El Rito Formation in the Tusas Mountains (Figure 3 and Appendix 1). At this location, there is an upsection decrease in clast size, and an increase in bed organization. Lithofacies transition from matrix- (predominately medium-coarse sand) and clast-supported disorganized conglomerate with boulders up to 2 m diameter at the base of the El Rito Formation to clast-supported, crudely horizontally bedded, imbricated cobble conglomerate at the top.

Galisteo depocenter trough cross-bedding ($N = 4$, $n = 74$) and primary current lineations ($N = 1$, $n = 13$) from this study generally show southwest-directed paleoflow (Figure 10a). However, when added to the more comprehensive dataset from Cather et al. (2002) there is a dominant southeast paleoflow direction for both the Diamond Tail and Galisteo formations (Figure 10a). These data indicate higher variability in the Galisteo Formation paleocurrent measurements compared to those of the Diamond Tail Formation. Paleocurrent measurements from the overlying Espinaso Formation exhibit exclusively west-directed sediment transport (Cather et al., 2002) (Figure 10a).

4.3 | Clast counts

Clast counts in the El Rito Formation confirm the previously documented dominance by quartzite clasts (Figure 10; Logsdon, 1981). In the Tusas Mountains, the El Rito Formation is entirely comprised of quartzite clasts (see Appendix 2). El Rito Formation clast counts in the eastern and western areas are dominated by quartzite as well (Figure 10b). After quartzite, vein quartz is the dominant clast type in the western area. In contrast, meta-rhyolite is the most dominant clast type after quartzite in the eastern area. Sedimentary clasts observed include sandstone, mudstone, conglomerate, and chert.

To the south, the Diamond Tail Formation clast count does not contain a greater variety, but does exhibit a more uniform distribution of clast types (Figure 7) in comparison to clast counts from the El Rito Formation. Vein quartz and quartzite are present in sub-equal proportions with subordinate chert and sandstone/mudstone clasts. Cather et al. (2002) report a dominance of limestone clasts for conglomerates at the base of the Galisteo Formation in the same area (i.e., Hagan area, Figure 3).

4.4 | Detrital zircon geochronology

4.4.1 | Mixing model

Mean Kuiper V values comparing measured samples to modeled mixtures range from 0.07–0.20 (Table 6). These Kuiper V values range from very good to poor (Saylor & Sundell, 2016), but most results generally yield adequate goodness of fit between mixed distributions and sample distribution. We interpret Kuiper V statistics <0.1 as a very good fit, the values in between 0.1 and 0.16 as ranging from good to moderately good, and ≥ 0.17 as a poor


(a)
(b)
(c)
Te
Jt
Jsm
Je
RWRT40
RWRT2
Tr
Te
Je
TRcf
(d)
Tg
Tdu
Tdm
~40 m
(e)
Tg
bedding plane
of rotated block
Tdu
interformational unconformity, dashed covered
formation contact, dashed covered
bedding plane strike and dip orientations
bedding dip
Tr Ritito Fm.
Te El Rito Fm.
Jsm Summersville/Morrison Fm.
Jt Todilto Fm.
Je Entrada Fm.
TRcf Chinle Fm., upper mb.

FIGURE 9 Field photos showing relevant field relationships. (a) Gravel dominated braided stream facies of the basal El Rito Formation in Arroyo del Cobre (36.241628°, −106.342789°). (b) Ribbed vertical burrows at ~24 m in the Red Wash Canyon measured section (36.246382°, −106.365371°). (c) High-relief basal unconformity of the El Rito Formation in Red Wash Canyon (36.245902°, −106.36687°). Yellow bar indicates approximate location of the Red Wash Canyon measured section (Figure 6). Also, approximate location of detrital zircon samples RWRT2 and RWRT40 are shown at the base and top of measured section (Figure 6) by black, zircon-shaped polygon. (d) View of the middle (Tdm) and upper (Tdu) members of the Diamond Tail Formation of the Galisteo depocenter (35.318577°, −106.305638°). Tg- Galisteo Formation. (e) Rotated block of sandstone at the top of the upper member of the Diamond Tail Formation, and directly below the Galisteo basal unconformity interpreted as a subaerial olistostrome (35.326141°, −106.305701°). Light blue strike and dip symbol indicates attitude of tilted block's bedding surface, which is dipping approximately toward the viewer (to the southeast). Light pink lines indicate bedding dip of surfaces approximately perpendicular to the image

fit. We report the source proportions and uncertainties based on the mean and standard deviation of the top 100 (0.1%) models ranked by V value. Uncertainties calculated in this way may approach the mean source proportions, particularly when source proportions are small. Our approach to interpreting mixture model results is to look for general trends, focus on larger source groups, disregard single source groups that exhibit low proportions and relatively high uncertainties, and incorporate multiple methods of detrital zircon data interpretation such as visual comparison of graphic representations and age range comparison.

4.4.2 | El Rito depocenter: Eastern and western study areas

Detrital zircon U-Pb age distributions from the base and top of the El Rito Formation show an upsection decrease in Cenozoic, Neoproterozoic, and Mesoproterozoic zircons accompanied by an increase in Paleoproterozoic (~1.7 Ga) zircon ages (Figure 11a–d). Samples from the lower El Rito Formation exhibit three subequal Proterozoic age modes (~1.7, ~1.4, and ~1.1 Ga), whereas samples from the upper El Rito Formation contain a dominant mode at ~1.7 Ga. Basal samples also contain larger proportions of younger (≤ 250 Ma, RWRT2 $n = 46$ and COB11 $n = 12$) detrital zircon ages than upper samples (RWRT40 $n = 7$ and 2ACRT40 $n = 7$). The basal sample (RWRT2) contains a notable population of Cenozoic zircons ($n = 23$), with a single-grain minimum age of 33.8 ± 1.2 (1σ) Ma, whereas the upper sample (RWRT40) contains only three Cenozoic zircons (YSG = 35.7 ± 1.3 (1σ) Ma). Eastern samples show similar results to those from the western area, but contain significantly fewer Cenozoic ages. Sample COB11 contains three Cenozoic zircons, with a minimum single-grain age of 37.6 ± 1.3 (1σ) Ma. Sample 2ACRT40 contains no ages younger than 100 Ma; the youngest detrital zircon age is 149.7 ± 6.25 (1σ) Ma. We present multiple methods of determining MDAs for samples that contain sufficient Cenozoic ages (Figure 8, Table 5), but rely on YSG method because of the relatively low number of analyzed grains (Coutts et al., 2019).

Relative source contributions yielded by *DZmix* modelling are consistent with qualitative observations described above. These results indicate that younger source groups (Triassic strata through Cretaceous–Cenozoic magmatic arc) provided most of the detritus for the basal El Rito Formation, whereas the Ortega Quartzite is the dominant source for the upper El Rito Formation (Figure 11a and c). Western and eastern samples from the basal El Rito Formation suggest different sourcing: the western sample is dominated by recycled Mesozoic eolianite and magmatic arc groups whereas the eastern sample indicates recycled early Cretaceous sourcing (Figure 11b and d). Kuiper V values for El Rito Formation samples and source profiles 1 and 1_SJ range from 0.09 to 0.016 (Table 6). Comparison of modeled and sample cumulative distribution functions (see Appendix 5) suggest that the primary mismatch is between sample Mesozoic–Cenozoic zircon populations and magmatic arc source attribution within the model. As with all samples analyzed in this study, the poorest model fits correspond to samples that contain the largest populations of Cenozoic zircons, indicating that we did not adequately characterize this source.

4.4.3 | Galisteo depocenter

Detrital zircon samples collected in this study that span the lower Diamond Tail through upper Galisteo formations, and previously published data from the Espinaso Formation (Sharman, Covault, Stockli, Wroblewski, & Bush, 2016) contain variable Cretaceous–Cenozoic zircon populations (Figure 11e–i). The lower and upper Diamond Tail formations contain few Cenozoic zircons ($n = 2$ for each), but their youngest single grain ages (62.3 ± 3.6 (1σ) and 54.9 ± 4.0 (1σ) Ma, respectively) are consistent with Paleocene–early Eocene depositional ages (Cather, 2004; Lucas et al., 1997). The lower Galisteo Formation records an increase in Mesozoic age proportion (25%) over both Diamond Tail Formation samples, but only contains one Cenozoic age zircon, which is older than the youngest age from the upper Diamond Tail Formation and so is not used as a depositional age. In contrast, two zircons from the upper Galisteo Formation sample yield ages of ~38 Ma (YSG = 38.4 ± 1.6 (1σ) Ma) and the youngest detrital zircon in the Espinaso

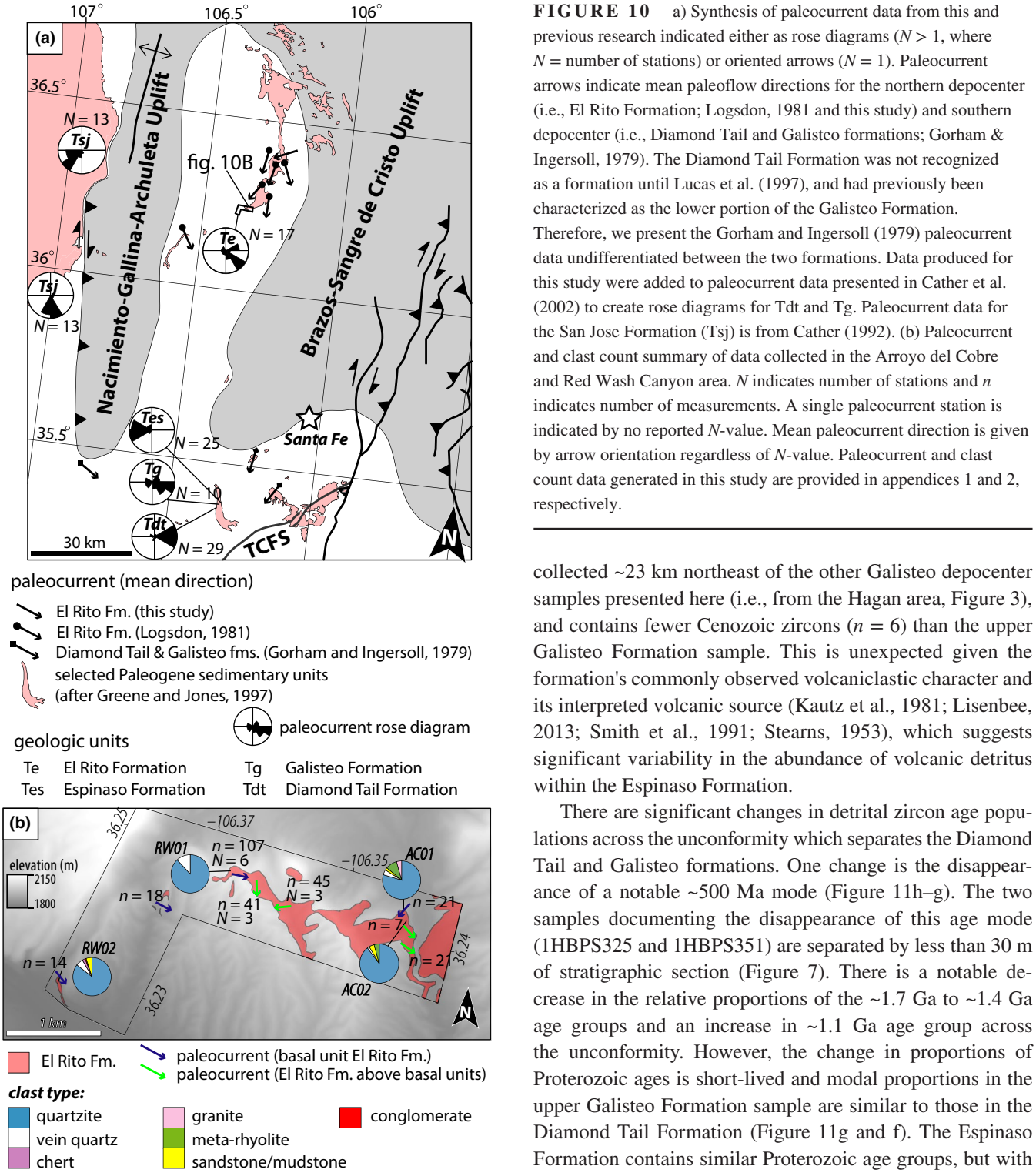

FIGURE 10 a) Synthesis of paleocurrent data from this and previous research indicated either as rose diagrams ($N > 1$, where N = number of stations) or oriented arrows ($N = 1$). Paleocurrent arrows indicate mean paleoflow directions for the northern depocenter (i.e., El Rito Formation; Logsdon, 1981 and this study) and southern depocenter (i.e., Diamond Tail and Galisteo formations; Gorham & Ingersoll, 1979). The Diamond Tail Formation was not recognized as a formation until Lucas et al. (1997), and had previously been characterized as the lower portion of the Galisteo Formation. Therefore, we present the Gorham and Ingersoll (1979) paleocurrent data undifferentiated between the two formations. Data produced for this study were added to paleocurrent data presented in Cather et al. (2002) to create rose diagrams for Tdt and Tg. Paleocurrent data for the San Jose Formation (Tsj) is from Cather (1992). (b) Paleocurrent and clast count summary of data collected in the Arroyo del Cobre and Red Wash Canyon area. *N* indicates number of stations and *n* indicates number of measurements. A single paleocurrent station is indicated by no reported *N*-value. Mean paleocurrent direction is given by arrow orientation regardless of *N*-value. Paleocurrent and clast count data generated in this study are provided in appendices 1 and 2, respectively.

Formation is 32.4 ± 0.6 (1σ) Ma (Table 5). All five samples exhibit multi-modal age distributions with varying modal proportions (Figure 11e–i). The most notable of these changes is the dearth of Cenozoic zircons in the lower three samples and the contrasting prevalence of this population in upper Galisteo Formation (3HBPS71 $n = 23$). The Espinaso Formation sample reported by Sharman et al. (2016) was collected ~23 km northeast of the other Galisteo depocenter samples presented here (i.e., from the Hagan area, Figure 3), and contains fewer Cenozoic zircons ($n = 6$) than the upper Galisteo Formation sample. This is unexpected given the formation's commonly observed volcaniclastic character and its interpreted volcanic source (Kautz et al., 1981; Lisenbee, 2013; Smith et al., 1991; Stearns, 1953), which suggests significant variability in the abundance of volcanic detritus within the Espinaso Formation.

There are significant changes in detrital zircon age populations across the unconformity which separates the Diamond Tail and Galisteo formations. One change is the disappearance of a notable ~500 Ma mode (Figure 11h–g). The two samples documenting the disappearance of this age mode (1HBPS325 and 1HBPS351) are separated by less than 30 m of stratigraphic section (Figure 7). There is a notable decrease in the relative proportions of the ~1.7 Ga to ~1.4 Ga age groups and an increase in ~1.1 Ga age group across the unconformity. However, the change in proportions of Proterozoic ages is short-lived and modal proportions in the upper Galisteo Formation sample are similar to those in the Diamond Tail Formation (Figure 11g and f). The Espinaso Formation contains similar Proterozoic age groups, but with subequal ~1.4 and ~1.7 Ga age modes. Finally, Paleozoic and Neoproterozoic age groups decrease from the lower Galisteo Formation through the Espinaso Formation.

The addition of the San Jose Formation conditional source group to source profile 1 (i.e., source profile 1_SJ; Figure 4) improved four out of five of the Galisteo depocenter sample mixture model results by decreasing their V statistics by an average of 0.021 (Table 6). In models with improved V statistics (i.e., lower and upper Diamond Tail, lower Galisteo,

TABLE 6 Kuiper V values for El Rito and Galisteo depocenters, and Gulf of Mexico samples for *DZmix* model runs for source profile 1 and both conditional source profiles

			Source profile 1		Source profile 1_SJ		Source profile 1_App		Source profile 1_App+SJ	
Depocenter		**Sample**	**V value**	**1σ**	**V value**	**1σ**	**V value**	**1σ**	**V value**	**1σ**
El Rito	West	*RWRT40*	0.125	±0.003	0.125	±0.003	n/a	n/a	n/a	n/a
		RWRT2	0.159	±0.006	0.161	±0.009	n/a	n/a	n/a	n/a
	East	*2ACRT40*	0.101	±0.004	0.105	±0.004	n/a	n/a	n/a	n/a
		COB11	0.09	±0.002	0.094	±0.004	n/a	n/a	n/a	n/a
Galisteo	*GB001*	0.134	±0.003	0.117	±0.004	n/a	n/a	n/a	n/a	n/a
	3HBPS71	0.169	±0.003	0.166	±0.002	n/a	n/a	n/a	n/a	n/a
	1HBPS351	0.114	±0.003	0.088	±0.003	n/a	n/a	n/a	n/a	n/a
	1HBPS325	0.112	±0.005	0.101	±0.002	n/a	n/a	n/a	n/a	n/a
	1HBPS10	0.101	±0.005	0.072	±0.005	n/a	n/a	n/a	n/a	n/a
Gulf of Mexico	Colorado-Brazos	*Vicksburg/Frio*	0.132	±0.000	0.132	±0.000	0.132	±0.000	0.132	±0.000
		Claiborne	0.166	±0.001	0.17	±0.001	0.075	±0.000	0.076	±0.004
		up Wilcox	0.203	±0.000	0.202	±0.001	0.203	±0.000	0.202	±0.001
		mid Wilcox	0.101	±0.002	0.098	±0.001	0.101	±0.001	0.100	±0.001
		low Wilcox	0.084	±0.002	0.084	±0.004	0.094	±0.004	0.090	±0.003
		Midway Gp.	0.096	±0.004	0.92	±0.002	0.095	±0.004	0.093	±0.003
	RG	*up Wilcox*	0.128	±0.000	0.124	±0.004	0.129	±0.001	0.125	±0.001
		low Wilcox	0.170	±0.004	0.172	±0.002	0.170	±0.004	0.171	±0.004

Abbreviation: Gp., Group.

and Espinaso formations), the San Jose Formation source group contributes 25% to 51% (Figure 11e, and g–i). Western Paleozoic and basement source groups constitute a significant portion of these models except for the lower Galisteo Formation. Instead, the lower Galisteo model shows low basement contribution and a correlative increase in Jurassic and Early Cretaceous source groups (Figure 11g). The upper Galisteo model fit is poor and statistically the same for both source group profiles 1 and 1_SJ. The model for this sample also indicates insignificant contribution from the San Jose Formation source group and exhibits significant magmatic arc sourcing (Figure 11f).

4.4.4 | Gulf of Mexico

Paleocene–Oligocene detrital zircon data are compiled from 18 samples from the paleo Colorado-Brazos fluvial system (Figure 2a, see Table 7 for references), and separated into 6 stratigraphic intervals: the early Paleocene Midway Group, the middle Paleocene lower Wilcox Group, the late Paleocene middle Wilcox Group, the early Eocene upper Wilcox Group, middle Eocene Claiborne Group, and early Oligocene Vicksburg/Frio Group. Detrital zircon spectra from five of six stratigraphic intervals exhibit similar proportions of Proterozoic populations at ~1.1, ~1.4, and ~1.7 Ga. Similarly, these data also contain a significant proportion of Mesozoic ages, with an upsection increase in both Mesozoic and Cenozoic age zircons (Figure 11j and K-O). In contrast, the middle Eocene Claiborne Group is dominated by ~1.1 Ga zircons, and contains fewer Mesozoic or Cenozoic ages than any other Gulf of Mexico sample presented here (Figure 11k).

Between the middle Wilcox and Vicksburg/Frio groups there are two significant changes in mixing model results (Figure 11l–j). The first is a decrease in western Paleozoic source and increase magmatic arc source between the middle and upper Wilcox Group. The upper Wilcox Group is the poorest fit of any models (V statistic = 0.2) indicating that no combination of potential sources adequately characterizes this stratigraphic interval. The second is the unique detrital zircon age distribution of the Claiborne Group sample, which also yielded poor model fits with our default source groups (V statistic = 0.17). However, when the conditional Appalachian source group was added as a potential sediment source (i.e., source profile 1_App, and source profile 1_App+SJ; Table 6), the Kuiper V value dropped to 0.08 while attributing ~65% of sourcing to the Appalachian group (Figure 11k). Conversely, the Appalachian source group is effectively absent from all other units. Finally, the Vicksburg/Frio Group model results return to similar pre-upper Wilcox Group proportions, while also yielding a 0.13 Kuiper V value.

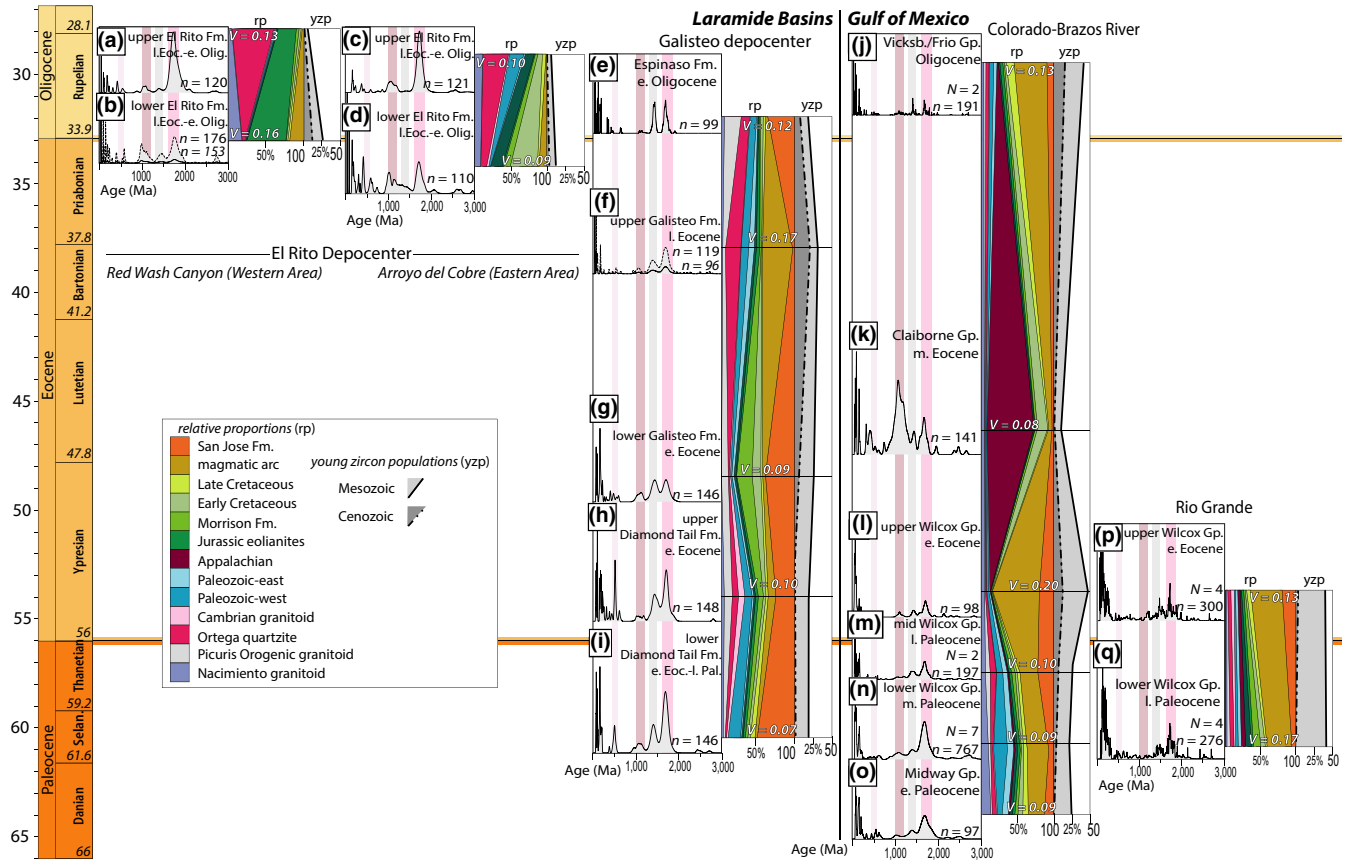

FIGURE 11 PDPs, DZmix calculated relative source proportions, and Cenozoic and Mesozoic populations for new and published Paleogene detrital zircon U-Pb data. Sample metadata is provided in Tables 4 and 7. The dashed lines in B and F are PDPs of that sample with the Cenozoic age zircons removed, and the resultant *n*-value is italicized. Vertical color bars on PDPs correspond to basement terranes described in Figure 4. DZmix relative proportions for the El Rito depocenter (a–d) are calculated from source 1, Galisteo depocenter relative proportions (e–i) are calculated from source 1_SJ, and Gulf of Mexico relative proportions (j–q) are calculated from source 1_App+SJ. Further detail of DZmix models is provided in Appendix 5. Numbers in relative source proportion columns are the Kuiper V statistic for the respective sample (Table 6). Names for El Rito and Galisteo depocenter samples commonly used in text, tables, figures, and appendices: A.-RWRT40, B.-RWRT2, C.-COB11, D.-2ACRT40, E.-GB001, F.-3HBPS71, G.-1HBPS351, H.-1HBPS325, I.-1HBPS10. E., early; Eoc., Eocene; Fm., Formation; Gp., Group; l., late; Olig., Oligocene; Pal, Paleocene; Vicksb., Vicksburg

Modeling source groups with the addition of the San Jose Formation source (i.e., source profile 1_SJ, and source profile 1_App+SJ; Table 6) produced similar results to source group 1 for Gulf of Mexico detrital zircon samples. Source profile 1_App+SJ mixing model results for Gulf of Mexico samples are consistent with the Galisteo depocenter model results (Figure 11).

Late Paleocene to earliest Eocene Rio Grande samples collected from the upper and lower Wilcox Group (Mackey, Horton, & Milliken, 2012) were compiled from 4 samples each and exhibit similar Proterozoic proportions described above for paleo Colorado-Brazos samples (excluding the Claiborne Group data). The Rio Grande data also contain significant Mesozoic populations (Figure 11p and Q, 40% and 37%, respectively). Mixture model results for source group 1_App+SJ indicate an upsection increase, from lower to upper Wilcox Group, in magmatic arc and San Jose Formation sources, while also exhibiting minor decreases in Mesozoic source groups. The mixing model closeness of fit for the paleo Rio Grande is consistently poor (V statistic = 0.17) for the lower Wilcox Group, and moderately good (V statistic = 0.12–0.13) for the upper Wilcox Group across all models (Table 6). These results indicate that our sources poorly characterize the Rio Grande's lower Wilcox Formation, and that the fluvial system feeding the San Jose Formation also may have contributed sediment the Rio Grande catchment during lower Wilcox deposition.

5 | DISCUSSION

5.1 | Sediment provenance

We make several general observations regarding application of *DZmix* to the detrital zircon data presented here.

TABLE 7 Summary of Gulf of Mexico detrital zircon geochronologic data used in this paper. Stratigraphic ages for Colorado-Brazos River samples assigned by cross-referencing Wahl et al. (2016) stratigraphy with Galloway et al. (2011) deposodes. Wahl et al. (2016) assign the Carrizo Formation sample (Cz) to the Claiborne Group, but we assign it to the upper Wilcox Group. Many researchers include the Carrizo Formation in the Wilcox Group (Hutto et al., 2009), and its early Eocene age assignment (Elisk & Crabaugh, 2001) is consistent with timing of Galloway et al.'s (2011) upper Wilcox deposode. Similarly, the late Paleocene Calvert Bluff Formation and late–middle Paleocene Simsboro, Hooper, and Seguin formations are consistent with the middle and lower Wilcox deposodes (Galloway et al., 2011), respectively, and were assigned to their corresponding groups

River	Sample names	Rock type	unit(s)	PDP figure	*N*	*n*	References
Colorado-Brazos	XOM-GOM 58, XOM-GOM 59	Sandstone	Vicksburg/Frio Group	Figure 8j	2	191	Blum et al. (2017)
	QC	Sandstone	Claiborne Group	Figure 8k	1	141	Blum et al. (2017)
	Cz	Sandstone	upper Wilcox Group	Figure 8l	1	98	Wahl et al. (2016)
	CB-BBM, CB-BS	Sandstone	mid Wilcox Group	Figure 8m	2	197	Wahl et al. (2016)
	Si-KM, Si-TQ, Si-LP, Si-B, H-DR, H-PC, Se	Sandstone	lower Wilcox Group	Figure 8n	7	767	Wahl et al. (2016)
	STeh	Sandstone	Midway Group	Figure 8o	1	97	Wahl et al. (2016)
Rio Grande	Z6, Z7, Z8,Z9	Sandstone	upper Wilcox Group	Figure 8p	4	300	Mackey et al. (2012)
	Z1, Z2, Z3, Z4	Sandstone	lower Wilcox Group	Figure 8q	4	276	Mackey et al. (2012)

Abbreviation: Gp., Group.

(a) Modelling provided insights into provenance changes that were not discernible through visual inspection of detrital zircon spectra (e.g., Galisteo depocenter provenance change across the inter-formational unconformity, Figure 11). Furthermore, mixture modelling provided a quantitative tool to differentiate source contribution between source spectra that share similar ages and proportions (e.g., Jurassic, Mesozoic eolianites, and Appalachian source groups). (b) Mixture modelling serves as a useful tool to refine potential source groups through iterative model runs and revisions to source profiles. (c) Modifying source groups yields insight into potential source variability, but is valid only when supported by independent geological observations. We found it useful to limit the number of source groups in the compilation, while still capturing the appropriate level of source diversity, and to balance that with as much consistency as possible across different depocenters. The modification of source profile 1 with two conditional source groups (i.e., source profile 1_SJ, source profile 1_App, and source 1_App+SJ) addresses these considerations.

5.2 | Age of the El Rito Formation

Detrital zircon MDAs indicate a latest Eocene–earliest Oligocene age for the El Rito Formation (Table 5), and provide a basis for regional correlations. Precise age assignment of the El Rito Formation has been problematic (Cather, 2004; Logsdon, 1981; Lucas, 1984; Lucas & Ingersoll, 1981), relying on "event stratigraphy" (Ager, 1973; Lucas, 1984), upper and lower bounding unconformities (Galusha & Blick, 1971; Lucas, 1984), or tenuous correlation to adjacent formations (Logsdon, 1981; Lucas, 1984; Lucas & Ingersoll, 1981; Yin & Ingersoll, 1997). The YSG for the basal western sample is 33.8 ± 1.2 (1σ) Ma in comparison to 37.6 ± 1.3 (1σ) Ma for the basal eastern sample, suggesting a westward delay in the onset of sedimentation between the eastern and western study areas (Figure 5). Although other methods of calculating MDA produce slightly older results for both samples, they consistently point to a latest Eocene–early Oligocene MDA with the onset of deposition at eastern area initiating 3–4 M.y. earlier than in the western area (Table 5, Figure 8). We prefer the YSG method for the samples presented here due to the low number of Paleogene age zircons, any one of which is probabilistically most likely to represent the modal age of a Gaussian distribution of ages approximating the depositional age (Coutts et al., 2019). The age of ~34 Ma for the basal El Rito Formation is consistent with a 32.3 ± 3.2 (1σ) youngest single grain MDA of the El Rito Formation in the Tusas Mountains (Donahue, 2016). However, these ages significantly revise the previously assigned early Eocene age for the basal El Rito Formation (Baltz, 1978; Logsdon, 1981; Lucas, 1984; Lucas & Ingersoll, 1981; Yin & Ingersoll, 1997) and have significant implications for its relationship to the Galisteo Formation (see *Basin synthesis* discussion below).

5.3 | El Rito depocenter: Sedimentological & stratigraphic trends

Provenance, paleocurrent, and lithofacies changes in the El Rito Formation consistently point to an upsection change

from a southward-flowing braided fluvial system fed by eastward-flowing tributaries and confined within narrow incised topography to a southward-flowing meandering river in a broad, intermontane alluvial plain (Figure 12b and c insets). The eastern and western measured sections both record upward-fining fluvial sequences with quartzite-clast-dominated, braided stream deposition at their base and sandy meandering stream deposition at the top. In the upper interval, the western section exhibits multiple well-developed paleosol intervals that contain pervasive terrestrial burrows (Figures 5 and 9b). These extended periods of pedogenic development are interpreted to have occurred during infilling of the BSC and NGA incised intermontane valley system, and were accompanied by a decrease in fluvial energy. Above this interval, channel sandstones exhibit evidence of lateral migration and flood plain cannibalization. Further change is indicated by paleocurrent indicators rotating from east-directed at the base of the western measured section to south- and west-directed in the upper portion of the section. At both measured section locations, an upsection switch from dominantly Mesozoic- to basement-derived detrital zircons is observed (Figure 11a–d). We interpret the basal El Rito unconformity and upsection changes in stratigraphy and provenance to chronicle the exhumation of the NGA Uplift and its subsequent waning influence over sedimentation in the El Rito depocenter by the late Eocene–early Oligocene. Furthermore, although not coeval with El Rito provenance trends, there is a similar upsection shift observed above the Diamond Tail-Galisteo unconformity where Mesozoic recycled sourcing is replaced by western Paleozoic and basement sources between the lower and upper Galisteo Formation (Figure 11g–f).

Provenance differences between the eastern and western study areas' lowermost samples in the El Rito depocenter point to subtly different source signatures, which give way upsection to a more uniform combination of sources. The greatest difference between the two locations of basal El Rito Formation detrital zircon data is the higher proportion of Mesozoic and Cenozoic zircons from the western compared to the eastern samples (Figure 11a–d). West-to-east and upsection decreases in Mesozoic and Cenozoic age zircons observed in the El Rito Formation are consistent with western-sourced zircons of these age groups which diminish in relative contribution through time. The upsection decrease in abundance of Mesozoic zircons is interpreted to reflect a diminishing of recycled Mesozoic strata mantling the NGA Uplift to the west. The upsection decrease in Cenozoic zircons suggests restriction of the El Rito catchment as it became isolated from increasingly proximal volcanic activity (Chapin et al., 2004).

The dominance of quartzite clasts in lower El Rito Formation conglomerates appears to contradict the detrital zircon results which suggest recycled Mesozoic source dominance within the same stratigraphic interval. However, the presence of these conglomerates (Figures 5 and 10b) provides insight into the source of quartzite gravels, and why they are associated with recycled Mesozoic detrital zircons. The absence of Proterozoic quartzite bedrock in the NGA Uplift (to the west) and its exposure in the BSC Uplift (to the east) (Jones et al., 2009) suggests that the quartzite gravels, at least in the east-flowing feeders, are recycled. An early Eocene, alluvial fan complex is proposed to have sourced the San Juan Basin from the BSC Uplift (Lucas, 1984). This alluvial fan would have partially mantled the incipient NGA Uplift and El Rito depocenter (Figure 13), and tapped basement lithologies exposed in the BSC Uplift (Baltz, 1967; Brister, 1992; Smith, 1992). We interpret the apparent provenance discrepancy between conglomerate clast counts and zircon geochronology in the lower El Rito Formation to reflect the relative mechanical robustness of quartzite clasts recycled from Eocene alluvial fan complex during exhumation of the NGA Uplift compared to the easily disaggregated Mesozoic strata stripped off the crest and eastern flank of the uplift.

West-flowing basement-clast conglomerates are preserved in the Llaves Member of the San Jose Formation (Smith, 1992), and are considered to be a northern example of a similar BSC-sourced fan complex as proposed above. However, the lack of coarse-grained detritus, including quartzite gravels, and the dominance of southward paleocurrent indicators in the San Jose Formation directly adjacent to the Nacimiento Uplift (Cather, 1992; Figure 10a) provide a maximum westward limit for the proposed alluvial fan. One possibility is that the quartzite alluvial fan that partially mantled the NGA Uplift transitioned into a finer grained fluvial system somewhere along the eastern flank of the incipient uplift as it was integrated into the well documented San Jose fluvial system. Another possibility is that earlier movement along the NGA Uplift (Baltz, 1967; Woodward, 1987) created a minor, but persistent drainage divide between the San Juan Basin and a precursor El Rito depocenter (Cather, 2004). The main phase of NGA exhumation (early Eocene) subsequently removed this stratigraphic record. Further detrital zircon work in the San Jose Formation may provide data to discriminate between the two models discussed above.

5.4 | Galisteo depocenter

Youngest single grain MDAs in the Galisteo depocenter are consistent with previously reported age control in these formations. For the basal and upper Diamond Tail Formation, YSGs (62.3 ± 3.6 (1σ) Ma and 54.9 ± 4.0 (1σ) Ma, respectively) match with rare mammalian fossils found in the middle of the formation that indicate early Eocene deposition (Lucas, 1982; Lucas & Williamson, 1993; Lucas et al., 1997). The same early Eocene fossils are also identified in

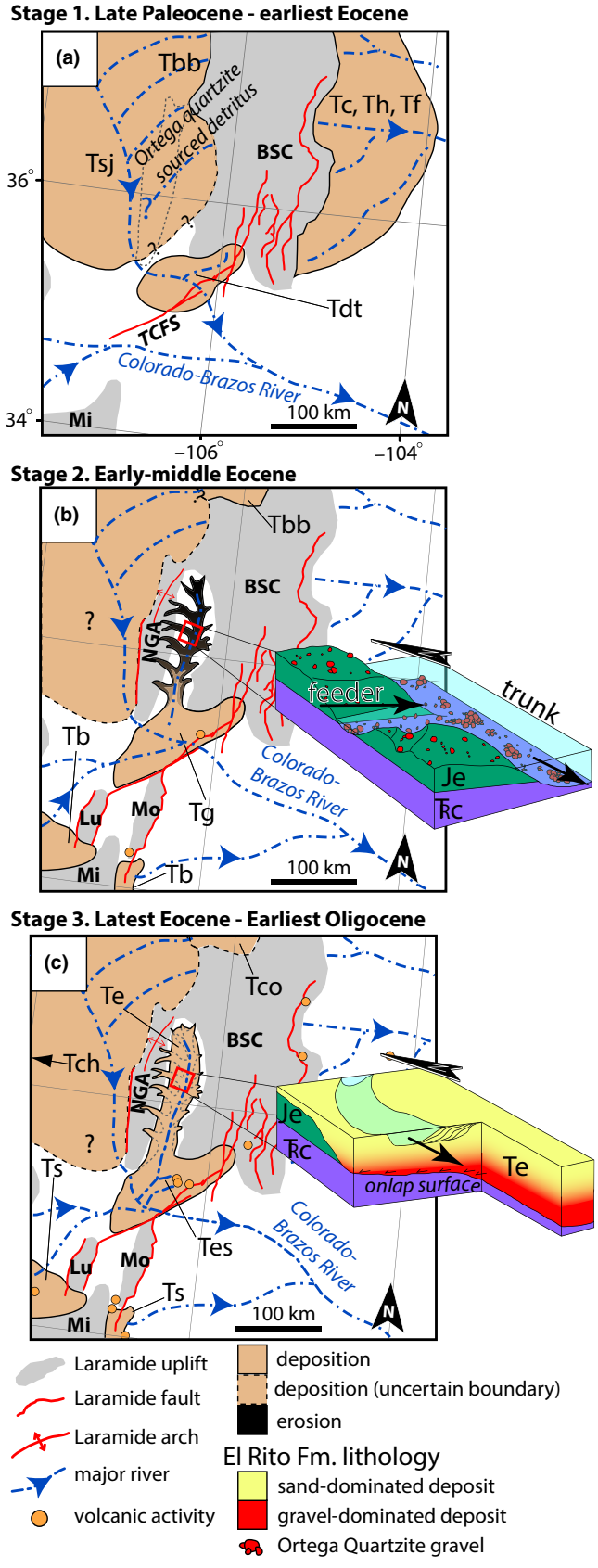

FIGURE 12 Three stage tectonic reconstruction of north-central New Mexico integrates local drainage changes within regional drainage networks (modified from Blum et al., 2017). (a) Late Paleocene and earliest Eocene fluvial networks that predate the primary phase of NGA rock and surface uplift, and exhumation (incipient position indicated by dashed grey line). This river system was sourced from a combination of northern (BSC Uplift) and western (San Juan Basin) sources and fed the paleo Colorado-Brazos River. (b) Following NGA exhumation and development of the inter-formational unconformity in the Galisteo depocenter in the early Eocene, deposition recommenced in the Galisteo depocenter. Upstream, erosion continued, resulting in formation of the high-relief basal unconformity of the El Rito Formation. The inset block diagram illustrates this bedrock river in the general vicinity of Red Wash Canyon and Arroyo del Cobre. Ortega Quartzite gravel was recycled from the west-flowing sediment transport systems illustrated in a). (c) Cessation of rock and surface uplift, and waning exhumation of the NGA resulted in decreased fluvial gradients, northward onlap by fluvial sediment into the incised topography, broadening of the fluvial system, and transition from gravel-dominated braided rivers to sand-dominated meandering rivers (shown in the block diagram). Dashed gray lines in the northern depocenter indicate buried incised topography. Arrow for the Tch indicates modern exposure of that formation, which is slightly west of map boundaries. Uplifts and faults: TCFS- Tijeras Cañoncito fault system, BSC- Brazos-Sangre de Cristo, NGA-Nacimiento-Gallina-Archuleta, Lu-Lucero, Mi-Morenci, Mo-Montosa. Formations organized by depocenter: El Rito depocenter: Je- Entrada Formation, TRc-Chinle Formation, Te-El Rito Formation; Galisteo depocenter: Tdt-Diamond Tail Formation, Tg- Galisteo Formation, Tes-Espinaso Formation; San Juan Basin: Tsj-San Jose Formation, Tbb- Blanco Basin Formation, Tch-Chuska Formation; Monte Vista Basin: Tbb-Blanco Basin Formation, Tco-Conejos Formation; Baca and Carthage La-Joya Basins: Tb- Baca Formation, Ts- Spears Formation. Uplift and basin geometries modified from Cather (2004) and Lawton (2008). Schematic fluvial pathways adapted from Cather (2004). Faults modified from Cather (2004) and Lisenbee (2013). Volcanic activity after Chapin et al. (2004)

the base of Galisteo Formation indicating that the intervening lacuna lasted no longer than 6 M.y. (Figure 13; Cather, 2004; Woodburne & Swisher, 1995). The age of the upper Galisteo Formation is ~38 Ma based on magnetostratigraphy (Prothero & Lucas, 1996). This is consistent with detrital zircon MDA from the upper Galisteo Formation (38.4 ± 1.6 (1σ) Ma, Table 6, Figure 8).

Provenance proxies provide insight into the nature of drainage reorganization across the basin-wide unconformity between the Diamond Tail and Galisteo formations in the Galisteo depocenter. Conglomerates directly above the unconformity contain a higher diversity of lithologies (e.g., sandstone, limestone, chert, granite, and quartzite) in comparison to the underlying Diamond Tail Formation (Cather et al., 2002; Gorham & Ingersoll, 1979). We attribute this increased clast variability to tectonic rejuvenation of NGA and portions of the BSC uplifts.

The change in detrital zircon age spectra, particularly the loss of the ~500 Ma age mode (Figure 11g to h), between the upper Diamond Tail and lower Galisteo formations is

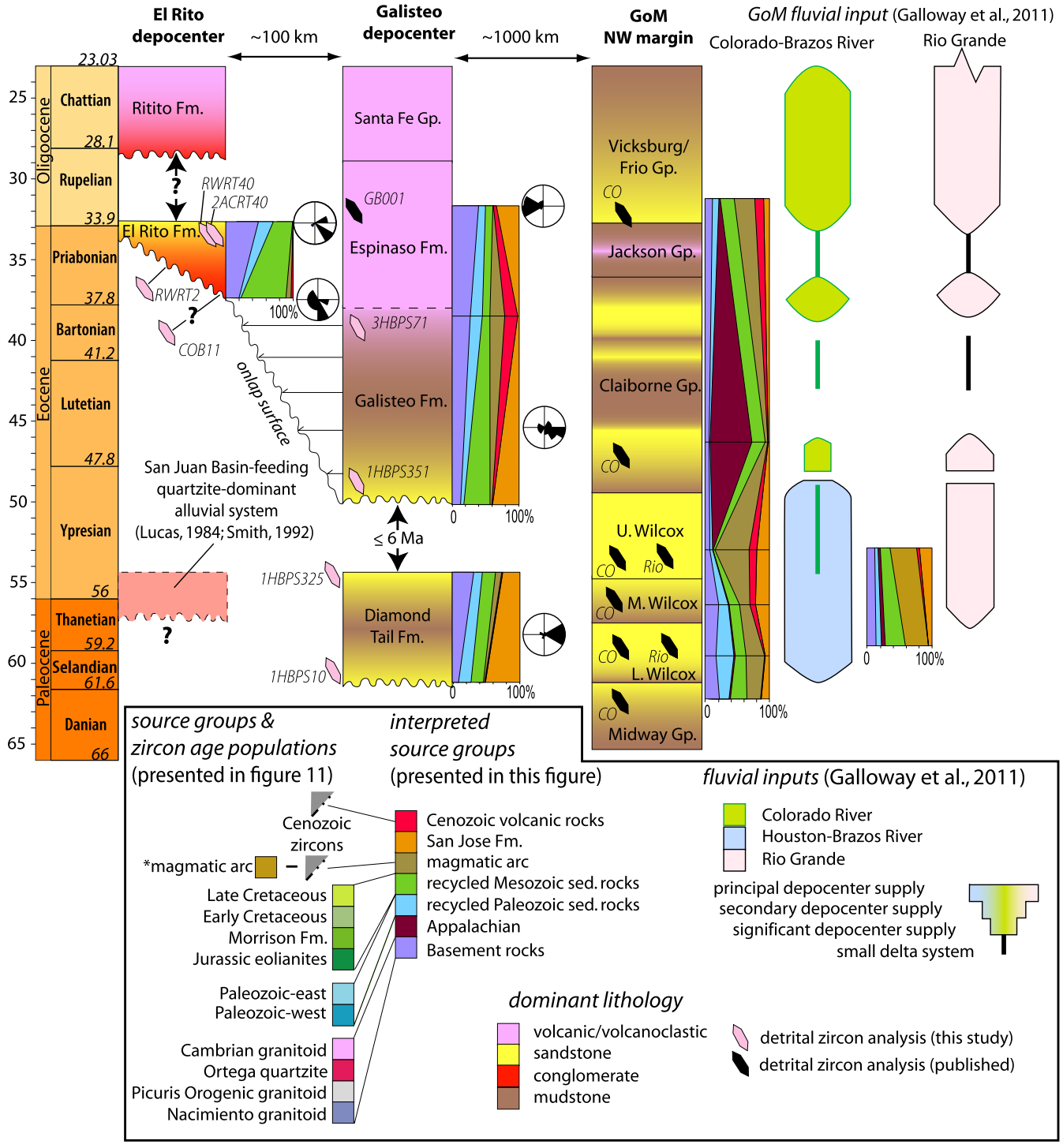

FIGURE 13 Chronostratigraphy, dominant lithologies, and interpreted source contributions for the El Rito depocenter, Galisteo depocenter, and the northwest margin of the Gulf of Mexico with approximate separation distances annotated between. Paleocurrent rose diagrams from Figure 10a are displayed in the appropriate stratigraphic position for the El Rito and Galisteo depocenter. Interpreted source contributions are created from modification of source contribution and young zircon population percentages presented in Figure 11 and illustrated in the figure key. Cenozoic volcanic rock interpreted source group is generated from the percentage of Cenozoic zircon population (Figure 11), which is subtracted from the magmatic arc group. The Espinaso Formation presents the one exception (indicated by the *) to this method as the percentage of Cenozoic zircons (6%) were greater than the magmatic arc source group attribution (3%). In this specific case we attribute the entire magmatic arc proportion to the Cenozoic volcanic zircon group, and allocate the remaining 3% from San Jose Formation source group. The depositional hiatus between the Diamond Tail and Galisteo formations is indicated by a gap in the source group interpretation column. Age control and facies information are provided by data presented herein and previously published data: Kautz et al. (1981), Lucas (1982), Kay (1986), Lucas and Williamson (1993), Woodburne and Swisher (1995), Prothero and Lucas (1996), Cather (2004), Maldonado and Kelley (2009), Lisenbee (2013), Cohen, Finney, Gibbard, and Fan (2013). Fm., Formation; Gp., Group; GoM., Gulf of Mexico; M., middle; L., lower; U., upper

indicative of tectonically-driven drainage reorganization (Figure 12a and b). We interpret the most likely source of ~500 Ma detrital zircons to be from the north or southeast. To the north, the Wet Mountains consistently supplied ~500 Ma zircons to the Huerfano Basin throughout the Paleocene and Eocene (Rasmussen & Foreman, 2017). It is possible that this drainage system also supplied ~500 Ma zircons to the Diamond Tail Formation via southwestward-flowing streams that were diverted after NGA exhumation. Alternatively, ~500 Ma zircons may have been sourced by late Cambrian-early Ordovician age igneous rocks of the Lobo and Pedernal hills (McMillan & McLemore, 2001), which are located ~50 and ~75 kilometers to the southeast, respectively (Figure 2). In either case, the disappearance of the ~500 Ma age mode indicates cessation of sedimentation from the north or southeast, and replacement by western-sourced rivers. The change in sediment sourcing was coeval with large-scale mass wasting (Figure 9e) and development of a regional unconformity at the base of the Galisteo Formation collectively supports the interpretation of tectonically driven drainage reorganization.

Similarities in provenance trends above the Diamond Tail-Galisteo unconformity and basal El Rito unconformity suggest that the two areas were affected by the same episode of tectonic activity: exhumation of the NGA Uplift. In both cases the Mesozoic source disappears or diminishes upsection, and is replaced by a source dominated by ~1.7 Ga zircon ages (primarily the Ortega Quartzite; Figures 4 and 11a–d, g, and f). The Mesozoic source is attributed to unroofing of Mesozoic formations during early-middle Eocene exhumation of the NGA Uplift (Figure 10a and b). The consistent San Jose Formation source group proportion observed through the Diamond Tail and lower Galisteo formations suggests a steady influence of this river system until deposition of the upper Galisteo Formation when the San Jose Formation source was almost completely replaced by magmatic arc source (Figure 11f). We interpret the increase in Cenozoic age zircons to account for the poor fit of magmatic arc source attribution (V statistic = 0.17) and to indicate local volcanic source contribution (Figures 12c and 13).

The Espinaso Formation records a westerly shift in paleocurrent indicators, which is attributed to a shift in fluvial gradients driven by the growth of the volcanic Ortiz Mountains and Cerrillos Hills to the east (Figures 3 and 12c). This is consistent with an increase in Picuris Orogenic granitoid source (~1.4 Ga), which is interpreted as basement sourced sediment from the BSC Uplift (e.g., Bush et al., 2016), while renewed of the San Jose Formation source group is best explained by recycling of Eocene fluvial sediments. The approximately 180° shift in paleoflow direction in the Hagan area (Figure 10a) and the relatively low abundance of Cenozoic volcanic-sourced detrital zircons to the north (Figures 3 and 11e) despite proximate development of at least two large volcanoes (Kautz et al., 1981) suggest that the Espinaso Formation was deposited during a time of drainage reorganization and expansion of highly localized catchments. Local changes in drainage networks most likely pushed the Colorado-Brazos River farther south than its position during the deposition of the Galisteo Formation. These drainage dynamics may have also exerted effects on deposition within the El Rito depocenter by affecting hydraulic gradients at the mouth of its fluvial corridor.

5.5 | Tectonic subsidence versus cut-and-fill accommodation of intermontane basins

Multiple lines of evidence support a tectonically-induced subsidence mechanism for the Galisteo depocenter. Diamond Tail and Galisteo stratigraphy thicken southwestward towards the Tijeras-Cañoncito fault system, and strike-oriented (northeast) paleocurrent indicators suggest that the fault zone exerted control over drainage patterns in the basin (Lisenbee, 2013). Paleocene kinematics along the Tijeras-Cañoncito fault system are obscured by prior and subsequent fault motion (Lisenbee, 2013). The specific mechanism of basin subsidence in this area is debated (i.e., transtensional vs. synclinal sag; Cather, 1992; Yin & Ingersoll, 1997, respectively), but stratigraphic thickness, basin geometry, proximity to the active Tijeras-Cañoncito fault system, and occurrence of mass-transport complexes directly beneath the Galisteo Formation basal unconformity (Figure 9e) support tectonic subsidence as the primary driver of accommodation in the Galisteo depocenter.

In contrast, the available geochronology, stratigraphy, and mapping indicates that accommodation for the El Rito Formation was created by tectonically-induced incision, rather than tectonic subsidence. The full thickness of the El Rito Formation in both Arroyo del Cobre and Red Wash Canyon area was deposited within the relief of the formation's basal unconformity (Figure 5). The El Rito Formation onlaps this high-relief basal unconformity (Figure 9c) suggesting a cut-and-fill accommodation mechanism for the El Rito Formation. Cut-and-fill accommodation is commonly found in intermontane basins (Hilley & Strecker, 2005), but until now, has not been invoked to explain preservation of the El Rito Formation.

5.6 | Laramide tectonics & geodynamics

We attribute the unconformity beneath the El Rito and Galisteo formations, and subsequent basin evolution, to the final stage of Laramide deformation. Initial movement of the NGA Uplift was minor and commenced in the Campanian (~78–75 Ma) based on thinning of the Lewis Shale across the Archuleta Anticlinorium (Cather, 2004; Gries, Clayton, & Leonard, 1997) and the thinning or absence of the ~75 Ma Pictured Cliffs Sandstone across the Nacimiento Uplift

(Baltz, 1967; Cather, 2004; Woodward, 1987). Synkinematic en echelon folds in the San Jose Formation record right-slip motion along the bounding fault zone of the NGA Uplift (Woodward, 1987) during the early Eocene, preceding the main phase of exhumation. However, data presented herein suggest that the majority of the approximately 2 km of Cretaceous and younger strata (Woodward, 1987) were removed from the Nacimiento Uplift (the primary and southern structural element of the NGA Uplift) as a result of early Eocene uplift and exhumation. The initiation of exhumation is constrained by the relatively short (≤6 M.y., Cather, 2004; Woodburne & Swisher, 1995) hiatus recorded between the Galisteo and Diamond Tail formations. This interpretation is consistent with timing of Nacimiento deformation observed in stratigraphic and structural relationships (Baltz, 1967; Woodward, 1987) as well as Eocene apatite fission track ages (Kelley et al., 1992).

The BSC Uplift was also active in the early Eocene, potentially experiencing exhumation coincident with and structurally linked to the NGA Uplift. The asymmetric basin geometry and eastward thickening of the Galisteo depocenter supports syndepositional tectonic activity along the eastern margin of the depocenter (Lisenbee, 2013). Further, dominant basement-clast cobble-boulder conglomerates, in some exposures of the Galisteo Formation (e.g., outcrops at St. Peter's Dome; Cather, 1992) support uplift of the BSC directly preceding or during Galisteo deposition. Along the eastern margin of the BSC Uplift, east-directed thrusting and folding affected early Eocene rocks of the Raton Basin (Cather, 2004; Johnson, 1959). This activity along the eastern and western margins of the BSC Uplift, in concert with NGA exhumation, are part of the terminal phase of Laramide tectonic activity.

Basins other than the Galisteo depocenter along the margin of the Laramide province were actively capturing sediment in the early to middle Eocene, reflecting a renewed episode of tectonic activity. Coarse-grained sediment was sequestered during this late stage of Laramide tectonic activity and preserved in the Denver Basin (Raynolds, 2002; Soister & Tschudy, 1978), Monte Vista Basin (Brister & Chapin, 1994), Echo Park Basin (Chapin & Cather, 1981), South Park Basin (Beggs, 1977; Chapin & Cather, 1983), Baca Basin (Cather, 2004), Carthage-La Joya Basin (Cather, 2009), Sierra Blanca Basin (Cather, 2009), and up to 1 km of strata in the San Juan Basin that has been subsequently eroded (Cather et al., 2003) (Figure 12b).

This final phase of Laramide-style deformation is coincident with proposed timing of initiation of Farallon slab rollback (Coney & Reynolds, 1977; Copeland et al., 2017; Dickinson & Snyder, 1978; Smith, Carroll, Jicha, Cassel, & Scott, 2014). The timing of north-central New Mexico deformation described herein, renewed Laramide basin accommodation, the increasing magnitude and punctuated nature of NGA associated deformation, and the subsequent increase in volcanic detritus observed in the upper Galisteo and Espinaso formations are consistent with models of multi-stage Laramide deformation during slab rollback (Cather, 2004; Chapin & Cather, 1983; Fan & Carrapa, 2014; Liu & Gurnis, 2010). These models point to accelerated upper plate deformation and westward migration of arc magmatism, and invoke upwelling of mantle and weakening of the North American plate due to slab rollback (Constenius, 1996; Fan & Carrapa, 2014; Humphreys et al., 2003).

5.7 | Basin Synthesis

We distill the proposed sequence of Paleogene tectonically-driven depositional events into three stages (Figure 12a–c). This synthesis proposes that tectonic activity along the NGA and potentially BSC uplifts drove local drainage reorganization and erosion that created the basal unconformity of the El Rito and Galisteo formations. Erosional truncation of underlying strata was followed by renewed subsidence in the south, and northward onlap of fluvial facies onto the unconformity. We interpret these stages within the context of proposed Paleogene transcontinental fluvial systems that drained into the Gulf of Mexico (Blum et al., 2017; Galloway et al., 2011).

5.7.1 | Stage 1: late Paleocene–earliest Eocene

During the late Paleocene and earliest Eocene, the headwaters of paleo Colorado-Brazos River occupied the future site of the El Rito and Galisteo depocenters (Blum et al., 2017; Galloway et al., 2011; Figure 12a). A fluvial system with a broad catchment and flowing through the San Juan Basin (Cather, 1992) delivered sediment to the Galisteo Basin during Diamond Tail deposition. The Llaves Member of the San Jose Formation records west-directed paleoflow and basement-sourced, gravel-dominated deposition (Smith, 1992), and lies to the north of the incipient NGA Uplift. Although not preserved in the rock record, similar alluvial fans extended south along the western flank of the BSC Uplift, tapping Ortega Quartzite, and partially mantling the incipient NGA Uplift (Lucas, 1984).

Local tectonic activity in the early Eocene drove formation of the unconformity that truncates the top Diamond Tail Formation and marks the end of Stage 1. Specifically, exhumation of the NGA Uplift, and renewed activity along the BSC Uplift and Tijeras-Cañoncito fault systems, induced subaerial mass wasting events recorded during the uppermost Diamond Tail Formation (Figure 9e), and resulted in development of a broad, regional unconformity at the base of the Galisteo and El Rito formations.

5.7.2 | Stage 2: early–middle Eocene

Resumption of sediment capture and deposition of the Galisteo Formation in the Galisteo depocenter marks the start of Stage 2 (Figure 12b). The increase in recycled Mesozoic material from the recently exhumed NGA Uplift and disappearance of the ~500 Ma detrital zircon mode indicate drainage reorganization across the basal Galisteo unconformity. Although deposition resumed in the Galisteo depocenter, our depositional chronology for the El Rito Formation indicates that the El Rito depocenter remained a zone of bypass or incision during Stage 2.

Return of accommodation in the Galisteo depocenter is mirrored by other Laramide basins around north-central New Mexico that also captured sediment during this stage. Although an unconformity in the San Juan Basin removed middle Eocene stratigraphy, approximately 1 km of middle Eocene-early Oligocene sedimentary rock is proposed to have been eroded (Cather et al., 2003). Fluvial to alluvial fan facies of the Blanco Basin Formation were deposited in newly developed Monte Vista Basin along the eastern margin of the San Juan Basin (Brister, 1992; Brister & Chapin, 1994) (Figure 12b). Fluvial and lacustrine facies of the Baca Formation were deposited in the Carthage-La Joya and Baca Basins (Cather, 2004) (Figure 12b).

The end of stage 2 is marked by the gradual increase of volcanic activity and volcaniclastic sediment capture in the region, the gradational transition from Galisteo Formation to Espinaso Formation deposition, and northward expansion of fluvial deposition from the Galisteo depocenter into the El Rito depocenter.

5.7.3 | Stage 3: late Eocene–early Oligocene

In the late Eocene, decreased fluvial gradients and sediment-transport capacity in the northern (i.e., El Rito Formation) depocenter resulted in transition from incision or bypass to sediment accumulation, and buried the incised landscape (Figure 12c). During this infilling process the remaining erosion-resistant gravels of Ortega Quartzite filled lower portions of feeder and trunk paleo-valleys. The more ephemeral tributary streams to the west experienced extended periods of pedogenesis following gravel deposition. As the El Rito trunk system aggraded, fluvial gradients decreased, and fluvial systems transitioned from braided to meandering (Schumm, 1981). The sand-dominated, meandering fluvial network was still confined by the incised valley, but the deepest and most constricting parts of the relief had been filled, thereby creating a broader intermontane fluvial plain that trended north-south between the BSC and NGA uplifts (Figure 12c).

MDAs provided by detrital zircons (Table 6, Figure 8) indicate that most, if not all, of the El Rito Formation was deposited while the Espinaso Formation was deposited in the Galisteo depocenter (Figure 12c). The volcanically active Ortiz Mountains and Cerrillos Hills, only several kilometers to the northeast, contributed abundant material to the Espinaso Formation (Kautz et al., 1981) while also receiving significant basement-derived zircons from the BSC Uplift. Despite proximity to active volcanism, the upper El Rito Formation records relatively little volcanic input. The greater abundance of Cenozoic zircons in the western samples suggests that they were delivered to the western reaches of the El Rito catchment via the distal edge of air-fall tuff(s). The dearth of Cenozoic volcanic zircons in the upper El Rito Formation (RWRT40 and 2ACRT40) and proximity to volcanically active locations (Figure 12c) also suggest that the El Rito catchment was topographically isolated from extrabasinal rivers that transported volcanic detritus post-peak tectonic uplift.

Sediment capture in surrounding Laramide depocenters that also sourced the headwaters of the Colorado-Brazos River system persisted during this stage. The Spears Formation in the Baca and Carthage-La Joya basins, as well the Conejos Formation around the Monte Vista Basin area captured detritus from local volcanic activity (Cather, 2004, 2009; Lipman, Steven, & Mehnert, 1970). Late Eocene fluvial rocks of the basal Chuska Formation record basement, recycled sedimentary, and volcanic sourcing in the western portion of the San Juan Basin, suggesting similar deposition in the axis of the basin despite subsequent erosion (Cather, 2009).

5.8 | The ultimate sink: Laramide activity & Gulf of Mexico sedimentation

Upstream changes in sediment character and storage impact downstream depocenters, but may be diluted and obscured through downstream integration with other rivers. This is evident in the dramatic provenance change and the extended period of erosion in the El Rito depocenter compared to the more subdued provenance change and abbreviated depositional hiatus in the Galisteo depocenter (Figure 12). These local source-to-sink systems are microcosms of the larger drainage systems linking the Laramide province and the Gulf of Mexico.

Paleogene fluvial systems draining northern New Mexico flowed to the Gulf of Mexico's northwest coast (Blum et al., 2017; Galloway et al., 2011). Peak sedimentation in the Gulf of Mexico occurred in the late Paleocene (Galloway et al., 2011). Peak sediment accumulation rate in the Gulf of Mexico approximately coincides with erosion and sediment bypass in many Laramide basins, including the Galisteo depocenter where it is marked by the basal Diamond Tail Formation unconformity (Cather, 2004; Dickinson et al., 1988). Conversely, some of the lowest Cenozoic sedimentation rates in the Gulf of Mexico occur in the middle Eocene and correspond to the timing of sediment capture in many

Laramide basins (e.g., Galisteo depocenter, Baca Basin, Sierra Blanca Basin, Carthage-la Joya Basin, Monte Vista Basin, Denver Basin, North Park Basin, Echo Park Basin; Cather, 2009; Cather et al., 2004; Chapin & Cather, 1983; Dickinson et al., 1988; Lawton, 2008; Soister & Tschudy, 1978).

Discrimination of sediment inputs from different Laramide source regions is complicated by abundant non-unique sources and coeval tectonic activity across the region. Further, even in sediment sourcing scenarios that involve unique detrital zircon age populations, recycling and downstream mixing may obfuscate provenance. Nevertheless, mixture model results from the Gulf of Mexico highlight detrital zircon ages that were missing (at least in the correct proportions) from our north-central New Mexico source profiles. Detrital zircon age populations of <200 Ma and >2.0 Ga from Gulf of Mexico samples are not characterized well by our source profiles. The former is the most significant contributor to the poor mixture model fits presented herein. We interpret the <200 Ma group to indicate sourcing from volcanic arc activity, which was focused along the western margin of North America, but was also distributed across much of the western interior during flat slab subduction and rollback (Coney & Reynolds, 1977; Copeland et al., 2017). Early Paleoproterozoic and Archean ages observed in the Gulf of Mexico dataset are most likely sourced from the northern Laramide province (i.e., WY and MT) where basement-cored structures exhumed rocks that range from 1.9 to 3.5 Ga (Chamberlain et al., 2003 and the references therein).

When comparing approximately coeval Gulf of Mexico and north-central New Mexico detrital zircon age distributions (Figure 10), it is important to interpret relative source increases and decreases within the context of mixture model comparison metrics. The good to very good fit of mixture models and similarity in non-magmatic arc source relative proportions between the Midway–middle Wilcox groups and the Diamond Tail Formation are consistent with similar sediment sourcing from north-central New Mexico in both source profiles 1 and 1_SJ (Table 6). We interpret the comparatively higher proportion of magmatic arc source and lower proportion of San Jose Formation source in the Gulf of Mexico samples to reflect downstream dilution by other in-route sediment source areas. The relatively poor model fit of the upper Wilcox Group sample indicates either poorly characterized source, which would indicate a change in the catchment during upper Wilcox deposition in the Colorado-Brazos catchment, or a poorly characterized basin sample due to the small sample size ($n = 98$).

Modelling the lower Claiborne Group with the Appalachian provenance group as a potential source (i.e., source group 1_App) significantly increases the goodness of fit compared to models that exclude the Appalachian provenance group (e.g., source group 1) (Table 6). Possible explanations for the significant change in detrital zircon age distribution during lower Claiborne Group deposition include two endmember scenarios: (a) recycling of Appalachian/Ouachita basin material (i.e., eastern source) or (b) recycling Mesozoic strata from the Laramide province (i.e., western source) (see Wahl, Yancey, Pope, Miller, & Ayers, 2016 for further discussion). We prefer the eastern-source interpretation from the Appalachian region for the following reasons: (a) the very good model fit of source profiles that included the Appalachian source group (V statistic = 0.08; source profiles 1_App and 1_App+SJ) versus the poor fit of source profiles without (V statistic = 0.17; source profiles 1 and 1_SJ) (Table 6), (b) the high proportion of Appalachian source (~65%; Figure 11k, Appendix 5) attributed to the Claiborne Group in models with a very good V statistic, (c) the observed decrease in an otherwise upward increasing trend in Mesozoic and Cenozoic zircons during Claiborne deposition (Figure 11k), (d) the change in the lower Claiborne Group's Proterozoic age proportions compared to the rest of the Paleocene–early Oligocene detrital zircon spectra (Figure 11j–o) despite waning basement-involved shortening during Claiborne deposition (i.e., middle Eocene) (Dickinson et al., 1988), and (e) the change in heavy mineral assemblage during this stratigraphic interval documented by other researchers (Craddock & Kylander-Clark, 2013; McCarley, 1981; Todd & Folk, 1957). We propose 3 possible eastern sources of Appalachian sediments to the lower Claiborne Group: (a) direct sourcing by Appalachian or Ouachita fluvial systems, (b) recycling of Appalachian-derived sediments from the Sabine Uplift during mid-Eocene exhumation (Ewing, 2009), or (c) local recycling of Appalachian-derived sediments from the Gulf coast. Regardless of the specific mechanism, the most salient control of lower Claiborne Group sediment composition is a decrease in Laramide province-sourced sediment in the middle Eocene (Galloway et al., 2011).

The westward incursion of Appalachian-derived source material along the Gulf of Mexico margin during Claiborne deposition, in part resulted from in-route storage of sediment by Laramide basins within the catchment of transcontinental drainage systems. The relative increase in Appalachian source contributions during the middle Eocene correlates with low sediment supply to the northwestern margin of the Gulf of Mexico (Eargle, 1968; Galloway, 2002; Galloway et al., 2011), and sediment capture by late stage Laramide basins such as the Galisteo depocenter. This overall decrease in sedimentation rate from Paleocene through Eocene (Galloway et al., 2011) occurs despite ongoing tectonism in the Laramide province and is a result of sequestration of sediment by Laramide basins. Waning tectonic activity during the middle to late Eocene decreased sediment production while pre-existing Laramide basins continued to sequester sediment, which further decreased external drainage. A dearth of Laramide-sourced detritus in the middle Eocene drove

multiple transgressions (Eargle, 1968) and westward incursion of eastern-derived sediment along the western margin of the Gulf of Mexico. This interpretation is consistent with Paleogene tectonic control of sediment delivery to the Gulf of Mexico (Sharman et al., 2016). Furthermore, it highlights the role of intraplate deformation-driven sediment capture within transcontinental drainage and the downstream effect on deposition within the receiving marine basin (i.e., ultimate sink). This implies a fundamental change in sediment character deposited along the western margin of the Gulf of Mexico during the middle Eocene, and reservoir quality of associated hydrocarbon systems.

6 | CONCLUSIONS

The El Rito and Galisteo formations were not coevally deposited nor do they share the same mechanism of accommodation. MDAs from detrital zircons along with previously published data indicate that most, if not all the Galisteo Formation predates deposition of the El Rito Formation (Table 5, Figure 8). Although we interpret the basal unconformity of the El Rito and Galisteo formations to be the same surface, their respective depocenters buried this unconformity at different times and are interpreted to have experienced fundamentally different accommodation mechanisms. While accommodation in the Galisteo depocenter was clearly driven by tectonic subsidence, the preservation of the El Rito Formation is attributed to incision and subsequent infilling of the erosional envelope created by exhumation of the NGA Uplift-driven river incision. This early Eocene exhumation was the primary driver local drainage reorganization and was generally coincident with regional drainage reorganization documented by Galloway et al. (2011) and Blum et al. (2017).

The western and eastern El Rito study areas are located at the junction between trunk and tributary streams in the El Rito fluvial system, which was bounded to east and west by the BSC and NGA uplifts, respectively. The lower El Rito Formation records a southward flowing trunk fluvial system with eastward flowing tributaries on its western flank. The lower El Rito Formation was deposited in the narrowest portion of these paleo-valleys. Paleocurrent measurements, detrital zircon data, and stratigraphic architecture indicate that during infilling of paleo-relief and broadening of the floodplain, the El Rito Formation transitioned from a gravelly braided system to sandy meandering system as local basement-involved tectonic activity waned, fluvial gradients flattened, and western-sourced feeder streams from the NGA Uplift receded.

Basal El Rito conglomerates and associated sandstones highlight discrepancies in provenance proxies and suggest recycling of BSC Uplift derived quartzite by the exhumation of the NGA Uplift. Conglomerates in the El Rito study area are consistently dominated by quartzite cobbles and boulders, yet associated detrital zircon age distributions, in agreement with paleocurrent data, reveal unique signatures from both the BSC and NGA uplifts, and suggest NGA Uplift sourcing. We interpret this disagreement to result from the difference in mechanical durability between the quartzite- and Mesozoic sandstone-derived gravels. Mobilization of recycled quartzite gravel alongside clasts of Mesozoic sandstone resulted in disaggregation of the weaker lithology and provenance biasing by grain size.

Early Eocene tectonic activity and associated drainage reorganization in north-central New Mexico exerted influence over sedimentation along the northwest margin of the Gulf of Mexico by restricting sediment to the paleo Colorado-Brazos River system. This was due at least in part to sediment sequestration during Eocene (e.g., Galisteo, El Rito, Espinaso, and Baca formations) deposition. Changes in drainage configuration and accommodation in these north-central New Mexico depocenters affected the distal reaches of Gulf of Mexico-bound fluvial systems through sediment production and capture, but were diluted and obscured through in-route sediment storage and downstream integration with other rivers. The middle Eocene decrease in sedimentation rates is coeval with a relative decrease in Laramide province-derived sediment and increase in Appalachian-derived sediment in the northwestern Gulf of Mexico margin. This suggests that sediment storage in Laramide basins played a first-order control on both the volume and character of the sediment delivered to the Gulf coast. This, in turn, impacted marine transgressions, stratal stacking patterns, and ultimately hydrocarbon prospectivity of Paleogene Gulf of Mexico reservoirs.

ACKNOWLEDGEMENTS

This study was by a gift from Chevron Corporation in support of a sedimentation and tectonics graduate-level field course at the University of Houston and by grants from the National Science Foundation (EAR-1742951 and EAR-1550097). Special thanks to Kurt Rudolph for field guidance and expert training. We thank Steve Cather and the unnamed reviewer for their thoughtful and constructive reviews. We also thank the editor of Basin Research, Cari Johnson, for her time, edits, and suggestions that she graciously provided in the handling of this manuscript, which has greatly benefited from the attention.

REFERENCES

Ager, D. (1973). *The nature of the stratigraphical record*. New York, NY: John Wiley and Sons Inc.

Amato, J., & Becker, T. (2012). Proterozoic rocks of the Caballo Mountains and Kingston mining district: U-Pb geochronology and

correlations within the Mazatzal Province of southern New Mexico. *New Mexico Geological Society Guidebook*, *63*, 227–234.

Amato, J. M., & Mack, G. H. (2012). Detrital zircon geochronology from the Cambrian-Ordovician Bliss Sandstone, New Mexico: Evidence for contrasting Grenville-age and Cambrian sources on opposite sides of the Transcontinental Arch. *Geological Society of America Bulletin*, *124*(11–12), 1826–1840. https://doi.org/10.1130/B30657.1

Averill, M. G., & Miller, K. C. (2013). Upper crustal structure of the southern Rio Grande rift: A composite record of rift and pre-rift tectonics. In M. R. Hudson & V. J. S. Grauch (Eds.), *New perspectives on Rio Grande Rift basins: From tectonics to groundwater* (pp. 463–474). Boulder, CO: Geological Society of America Special Paper 494.

Baltz, E. H. (1965). Stratigraphy and history of the Raton basin and notes on the San Luis basin. Colorado-New Mexico. *American Association Petroleum Geologists*, *49*(11), 2041–2075.

Baltz, E. H. (1967). *Stratigraphy and regional tectonic implications of part of Upper Cretaceous and Tertiary rocks, east-central San Juan Basin, New Mexico*. US Govt. Printing Office, 2330-7102.

Baltz, E. H. (1978). Resume of Rio Grande depression in north-central New Mexico. Guidebook to the Rio Grande Rift. *Circular*, *63*, 210–226.

Becker, T. P., Thomas, W. A., Samson, S. D., & Gehrels, G. E. (2005). Detrital zircon evidence of Laurentian crustal dominance in the lower Pennsylvanian deposits of the Alleghenian clastic wedge in eastern North America. *Sedimentary Geology*, *182*(1), 59–86. https://doi.org/10.1016/j.sedgeo.2005.07.014

Becker, T. P., Thomas, W. A., & Gehrels, G. E. (2006). Linking late Paleozoic sedimentary provenance in the Appalachian basin to the history of Alleghenian deformation. *American Journal of Science*, *306*(10), 777–798.

Beggs, H. G. (1977). Interpretation of seismic reflection data from the central South Park Basin, Colorado. In H. K. Veal (Ed.), *Exploration frontiers of the central and southern Rockies* (pp. 67–76). Denver, CO: Rocky Mountain Association of Geologists.

Bingler, E. C. (1968). Geology and mineral resources of Rio Arriba County, New Mexico. *New Mexico Bureau of Mines and Mineral Resources Bulletin*, *91*, 157.

Blum, M. D., Milliken, K. T., Pecha, M. A., Snedden, J. W., Frederick, B. C., & Galloway, W. E. (2017). Detrital-zircon records of Cenomanian, Paleocene, and Oligocene Gulf of Mexico drainage integration and sediment routing: Implications for scales of basin-floor fans. *Geosphere*, *13*(6), 2169–2205. https://doi.org/10.1130/GES01410.1

Brister, B. S., & Chapin, C. E. (1994). Sedimentation and tectonics of the Laramide San Juan sag, southwestern Colorado. *The Mountain Geologist*, *31*(1), 2–18.

Brister, B. S. (1992). The Blanco Basin Formation (Eocene), San Juan Mountains region, Colorado and New Mexico. *New Mexico Geological Society Guidebook*, 43rd Field Conference, San Juan Basin IV, 321–331.

Bush, M. A., Horton, B. K., Murphy, M. A., & Stockli, D. F. (2016). Detrital record of initial basement exhumation along the Laramide deformation front, southern Rocky Mountains. *Tectonics*, *35*(9), 2117–2130. https://doi.org/10.1002/2016TC004194

Cardozo, N., & Allmendinger, R. W. (2013). Spherical projections with OSXStereonet. *Computers & Geosciences*, *51*, 193–205. https://doi.org/10.1016/j.cageo.2012.07.021

Cather, S. M. (1990). Stress and volcanism in the northern Mogollon-Datil volcanic field, New Mexico: Effects of the post-Laramide tectonic transition. *Geological Society of America Bulletin*, *102*(11), 1447–1458. https://doi.org/10.1130/0016-7606(1990)102<1447:SAVITN>2.3.CO;2

Cather, S. M. (1992). Suggested revisions to the Tertiary tectonic history of north-central New Mexico: San Juan Basin IV. *New Mexico Geological Society Guidebook*, *43*, 109–122.

Cather, S. M. (2004). Laramide orogeny in central and northern New Mexico and southern Colorado: The Geology of New Mexico, A Geologic History. *New Mexico Geological Society Special Publication*, *11*, 203–248.

Cather, S. M. (2009). Stratigraphy and structure of the Laramide Carthage-La Joya Basin, central New Mexico. *New Mexico Geological Society*, 60th Field Conference, Guidebook, 227–234.

Cather, S. M., Connell, S. D., Lucas, S. G., Picha, M. G., & Black, B. A. (2002). Geologic map of the Hagan quadrangle, Santa Fe county, New Mexico. *New Mexico Bureau of Geology and Mineral Resources*, Open File-Geologic Map 050.

Cather, S. M., Peters, L., Dunbar, N. W., & McIntosh, W. C. (2003). Genetic stratigraphy, provenance, and new age constraints for the Chuska Sandstone. *New Mexico-Arizona: New Mexico Geological Society*, 54th Field Conference, Guidebook, 397–412.

Chamberlain, K. R., Frost, C. D., & Frost, B. R. (2003). Early Archean to Mesoproterozoic evolution of the Wyoming Province: Archean origins to modern lithospheric architecture. *Canadian Journal of Earth Science*, *40*, 1357–1374.

Chapin, C. E., & Cather, S. M. (1981). Eocene tectonics and sedimentation in the Colorado Plateau-Rocky Mountain area: Relations of tectonics to ore deposits in the southern Cordillera. *Arizona Geological Society Digest*, *14*, 173–198.

Chapin, C. E., & Cather, S. M. (1983). Eocene tectonics and sedimentation in the Colorado Plateau Rocky Mountain area. In J. D. Lowell (Ed.), *Rocky Mountain foreland basins and uplifts* (pp. 33–56). Denver, CO: Rocky Mountain Association of Geologists.

Chapin, C. E., Wilks, M., & McIntosh, W. C. (2004). Space-time patterns of Late Cretaceous to present magmatism in New Mexico-Comparison with Andean volcanism and potential for future volcanism. *New Mexico Bureau of Geology and Mineral Resources Bulletin*, *160*, 13–40.

Clark, K. (1966). Geology of the Sangre de Cristo Mountains and adjacent areas between Taos and Raton. New Mexico. *New Mexico Geological Society Guidebook*, *17*, 56–65.

Clift, P. D., Blusztajn, J., & Nguyen, A. D. (2006). Large-scale drainage capture and surface uplift in eastern Tibet-SW China before 24 Ma inferred from sediments of the Hanoi Basin. *Vietnam. Geophysical Research Letters*, *33*, 1–5. https://doi.org/10.1029/2006GL027772

Clinkscales, C. A., & Lawton, T. F. (2015). Timing of Late Cretaceous shortening and basin development, Little Hatchet Mountains, southwestern New Mexico, USA-implications for regional Laramide tectonics. *Basin Research*, *27*, 453–472. https://doi.org/10.1111/bre.12083

Cohen, K. M., Finney, S. C., Gibbard, P. L., & Fan, J. X. (2013). The ICS international chronostratigraphic chart. *Episodes*, *36*(3), 199–204.

Coney, P. J., & Reynolds, S. (1977). Cordilleran Benioff zones. *Nature*, *270*(5636), 403–406. https://doi.org/10.1038/270403a0

Constenius, K. N. (1996). Late Paleogene extensional collapse of the Cordilleran foreland fold and thrust belt. *GSA Bulletin*, *108*(1), 20–39.

Copeland, P., Currie, C. A., Lawton, T. F., & Murphy, M. A. (2017). Location, location, location: The variable lifespan of the Laramide orogeny. *Geology*, *45*(3), 224–226. https://doi.org/10.1130/G38810.1

Coutts, D., Matthew, W., & Hubbard, S. (2019). Assessment of widely used methods to derive depositional ages from detrital zircon populations. *Geoscience Frontiers*. https://doi.org/10.1016/j.gsf.2018.11.002 (in press).

Craddock, W. H., & Kylander-Clark, A. R. (2013). U-Pb ages of detrital zircons from the Tertiary Mississippi River Delta in central Louisiana: Insights into sediment provenance. *Geosphere*, *9*, 1832–1851. https://doi.org/10.1130/GES00917.1

Daniel, C. G., Pfeifer, L. S., Jones III, J. V., & McFarlane, C. M. (2013). Detrital zircon evidence for non-Laurentian provenance, Mesoproterozoic (ca. 1490–1450) deposition and orogenesis in a constructed orogenic belt, northern New Mexico, USA: Defining the Picuris orogeny. *Geological Society of America Bulletin*, *125*(9/10), 1423–1441.

Davis, S. J., Wiegand, B. A., Carroll, A. R., & Chamberlain, C. P. (2008). The effect of drainage reorganization on paleoaltimetry studies: An example from the Paleogene Laramide foreland. *Earth and Planetary Science Letters*, *275*, 258–268. https://doi.org/10.1016/j.epsl.2008.08.009

Decelles, P. G. (2004). Late Jurassic to Eocene evolution of the Cordilleran thrust belt and foreland basin system, western USA. *American Journal of Science*, *304*(2), 105–168. https://doi.org/10.2475/ajs.304.2.105

Decelles, P. G., Langford, R. P., & Schwartz, R. K. (1983). Two new methods of paleocurrent determination from trough cross-stratification. *Journal of Sedimentary Research*, *53*, 2.

Dickinson, W. R., Klute, M. A., Hayes, M. J., Hanecke, S. U., Lundin, E. R., McKittrick, M. A., & Olivares, M. D. (1988). Paleogeographic and paleotectonic setting of Laramide sedimentary basins in the central Rocky Mountain region. *Geological Society of American Bulletin*, *100*, 1023–1039. https://doi.org/10.1130/0016-7606(1988)100<1023:PAPSOL>2.3.CO;2

Dickinson, W. R., & Gehrels, G. E. (2003). U-Pb ages of detrital zircons from Permian and Jurassic eolian sandstones of the Colorado Plateau, USA: Paleogeographic implications. *Sedimentary Geology*, *163*(1–2), 29–66. https://doi.org/10.1016/S0037-0738(03)00158-1.

Dickinson, W. R., & Gehrels, G. E. (2008a). Sediment delivery to the Cordilleran foreland basin: Insights from U-Pb ages of detrital zircons in Upper Jurassic and Cretaceous strata of the Colorado Plateau. *American Journal of Science*, *308*(10), 1041–1082.

Dickinson, W. R., & Gehrels, G. E. (2008b). U-Pb ages of detrital zircons in relation to paleogeography: Triassic paleodrainage networks and sediment dispersal across southwest Laurentia. *Journal of Sedimentary Research*, *78*, 745–764. https://doi.org/10.2110/jsr.2008.088

Dickinson, W. R., & Gehrels, G. E. (2009). Use of U-Pb ages of detrital zircons to infer maximum depositional ages of strata: A test against a Colorado Plateau Mesozoic database. *Earth and Planetary Science Letters*, *288*, 115–125. https://doi.org/10.1016/j.epsl.2009.09.013

Dickinson, W. R., & Snyder, W. S. (1978). Plate tectonics of the Laramide orogeny. In V. Matthews., III, (Ed.), *Laramide Folding Associated with Basement Block Faulting in the Western United States: Geological Society of America Memoir 151* (pp. 355–366).

Donahue, M. M. (2016). *Episodic Uplift of the Rocky Mountains: Evidence from U-Pb detrital zircon geochronology and low-temperature thermochronology with a chapter on using mobile technology for geoscience education* (Ph.D. thesis). University of New Mexico, Albuquerque.

Dyman, T. S., Tysdal, R. G., Perry, W. J. J., Nichols, D. J., & Obradovich, J. D. (2008). Stratigraphy and structural setting of Upper Cretaceous frontier formation, western Centennial Mountains, southwestern Montana and southeastern Idaho. *Cretaceous Research*, *29*(2), 237–248. https://doi.org/10.1016/j.cretres.2007.05.001.

Eargle, D.H. (1968). Nomenclature of formations of Claiborne Group, Middle Eocene coastal plain of Texas, United States Geological Survey Bulletin 1251-D, United States Printing Office, Washington D.C.

Elsik, W. C., & Crabaugh, J. P. (2001). Palynostratigraphy of the upper Paleocene and lower Eocene Wilcox Group in the northwestern Gulf of Mexico basin. In D. K. Goodman & R. T. Clarke (Eds.), *Proceedings of the IX International Palynological Congress, Houston, Texas* (pp. 233–237). Baton Rouge, Louisiana: American Association of Palynologists Foundation.

Erslev, E. A. (2001). Multistage, multidirectional Tertiary shortening and compression in north-central New Mexico. *Geological Society of America Bulletin*, *113*(1), 63–74. https://doi.org/10.1130/0016-7606(2001)113<0063:MMTSAC>2.0.CO;2

Ewing, T. E. (2009). The ups and downs of Sabine Uplift and Gulf of Mexico basin: Jurassic basement blocks, Cretaceous thermal uplifts, and Cenozoic. *Gulf Coast Association of Geological Societies Transactions*, *59*, 253–269.

Fan, M., & Carrapa, B. (2014). Late Cretaceous-early Eocene Laramide uplift, exhumation, and basin subsidence in Wyoming: Crustal responses to flat slab subduction. *Tectonics*, *33*, 509–529. https://doi.org/10.1002/2012TC003221

Galloway, W. E. (2002). Cenozoic evolution of sediment accumulation in deltaic and shore-zone depositional systems, northern Gulf of Mexico Basin. *Marine and Petroleum*, *18*, 1031–1040. https://doi.org/10.1016/S0264-8172(01)00045-9

Galloway, W. E., Whiteaker, T. L., & Ganey-Curry, P. (2011). History of Cenozoic North American drainage basin evolution, sediment yield, and accumulation in the Gulf of Mexico basin. *Geosphere*, *7*(4), 938–973. https://doi.org/10.1130/GES00647.1

Galusha, T., & Blick, J. C. (1971). Stratigraphy of the Santa Fe Group, New Mexico. *American Museum of Natural History Bulletin*, *144*, 7–127.

Gehrels, G. E., Valencia, V. A., & Ruiz, J. (2008). Enhanced precision, accuracy, efficiency, and spatial resolution of U-Pb ages by laser ablation–multicollector-inductively coupled plasma–mass spectrometry. *Geochemistry, Geophysics, Geosystems*, *9*(3), 1–13. https://doi.org/10.1029/2007GC001805

Gorham, T. W. (1979). *Geology of the Galisteo Formation: Hagan basin, New Mexico* (MS thesis). University of New Mexico, Albuquerque.

Gorham, T. W., & Ingersoll, R. V. (1979). Evolution of the Eocene Galisteo basin, north-central New Mexico: Santa Fe country. *New Mexico Geological Society Guidebook*, *30*, 219–224.

Green, G. N., & Jones, G. E. (1997). The digital geologic map of New Mexico in ARC/INFO format. U.S. Geological Survey Open-File Report 97-0052.

Gries, R. (1983). North-south compression of Rocky Mountain foreland structures. In J. D. Lowell & R. Gries (Eds.), *Rocky Mountain foreland basins and uplifts* (pp. 9–32). Denver, CO: Rocky Mountain Association of Geologists.

Gries, R. R., Clayton, J. L., & Leonard, C. (1997). Geology, thermal maturation, and source rock geochemistry in a volcanic covered basin: San Juan Sag, south-central Colorado. *American Association of Petroleum Geologists Bulletin*, *81*, 1133–1160.

Hilbert-Wolf, H., Roberts, E., Downie, B., Mtelela, C., Stevens, N. J., & O'Conner, P. (2017). Application of U-Pb detrital zircon geochronology to drill cuttings for age control in hydrocarbon exploration wells: A case study from the Rukwa Rift Basin, Tanzania. *American Association of Petroleum Geologist Bulletin*, *101*(2), 143–159. https://doi.org/10.1306/06281616003

Hilley, G. E., & Strecker, M. R. (2005). Processes of oscillatory basin filling and excavation in a tectonically active orogen: Quebrada del Toro Basin, NW Argentina. *Geological Society of America Bulletin*, *117, 7(8)*, 887–901. https://doi.org/10.1130/B25602.1

Hudson, M. R., & Grauch, V. J. S. (2013). Introduction. In M. R. Hudson & V. J. S. Grauch (Eds.), *New perspectives on Rio Grande Rift basins: From tectonics to groundwater* (pp. 5–12). Geological Society of America Special Paper, 494.

Humphreys, E. (2009). Relation of flat subduction to magmatism and deformation in the western United States. *Geological Society of America Memoirs*, *204*, 85–98.

Humphreys, E., Hessler, E., Dueker, K., Farmer, G. L., Erslev, E., & Atwater, T. (2003). How Laramide-age hydration of North American lithosphere by the Farallon slab controlled subsequent activity in the western United States. *International Geology Review*, *45*(7), 575–595. https://doi.org/10.2747/0020-6814.45.7.575

Hutto, A. P., Yancey, T. E., & Miller, B. V. (2009). Provenance of Paleocene-Eocene Wilcox Group sediments in Texas: The evidence from detrital zircons. *Gulf Coast Association of Geological Societies Transactions*, *59*, 357–362.

Ingersoll, R. V., Cavazza, W., Baldridge, W. S., & Shafiqullah, M. (1990). Cenozoic sedimentation and paleotectonics of north-central New Mexico: Implications for initiation and evolution of the Rio Grande rift. *Geological Society of America Bulletin*, *102*, 1280–1296. https://doi.org/10.1130/0016-7606(1990)102<1280:CSAPON>2.3.CO;2

Johnson, R. B. (1959). Geology of the Huerfano Park area, Huerfano and Custer Counties, Colorado. *U.S. Geological Survey Bulletin*, *1071-D*, C87–C119.

Jones III, J. V., Connelly, J. N., Karlstrom, K. E., Williams, M. L., & Doe, M. F. (2009). Age, provenance, and tectonic setting of Paleoproterozoic quartzite successions in the southwestern United States. *Geological Society of America Bulletin*, *121*(1–2), 247–264.

Jones III, J. V., Daniel, C. G., Frei, D., & Thrane, K. (2011). Revised regional correlations and tectonic implications of Paleoproterozoic and Mesoproterozoic metasedimentary rocks in northern New Mexico, USA: New findings from detrital zircon studies of the Hondo Group, Vadito Group, and Marquenas Formation. *Geosphere*, *7*(4), 974–991. https://doi.org/10.1130/GES00614.1

Karlstrom, K. E., & Bowring, S. A. (1988). Early Proterozoic assembly of tectonostratigraphic terranes in southwestern North America. *The Journal of Geology*, *96*, 561–576. https://doi.org/10.1086/629252

Karlstrom, K. E., & Humphreys, E. D. (1998). Persistent influence of Proterozoic accretionary boundaries in the tectonic evolution of southwestern North America. *Rocky Mountain Geology*, *33*(2), 161–179.

Kautz, P. F., Ingersoll, R. V., Baldridge, W. S., Damon, P. E., & Shafiqullah, M. (1981). Geology of Espinaso Formation (Oligocene), north-central New Mexico. *Geological Society of America Bulletin*, *92*, 2318–2400.

Kay, B. (1986). *Vein and breccia gold mineralization and associated igneous rocks at the Ortiz mine: New Mexico, USA* (MS thesis). Colorado School of Mines, Golden, CO.

Kelley, S. A., Chapin, C. E., & Corrigan, J. (1992). Late Mesozoic to Cenozoic cooling histories of the flanks of the northern and central Rio Grande rift, Colorado and New Mexico. *New Mexico Bureau of Mines and Mineral Resources Bulletin*, *145*, 5–33.

Kelley, S.A., Osburn, G.R., Ferguson, C., Moore, J., & Kempter, K. (2005). Geology of the Cañones 7.5-Minute quadrangle, Rio Arriba County, New Mexico: New Mexico Bureau of Geology and Mineral Resources, Open-file Geologic Map OF-GM 107, scale 1:24,000.

Kuiper, N. H. (1960). Tests concerning random points on a circle. *Indagationes Mathematicae*, *63*, 38–47. https://doi.org/10.1016/S1385-7258(60)50006-0

Laskowski, A. K., Decelles, P. G., & Gehrels, G. E. (2013). Detrital Zircon geochronology of Cordilleran retroarc foreland basin strata, western North America. *Tectonics*, *32*, 1027–1048. https://doi.org/10.1002/tect.20065

Lawton, T. F. (2008). Laramide sedimentary basins. In A. D. Miall (Ed.), *Sedimentary basins of the world* (Vol. *5*, pp. 429–450). Netherlands: Elsevier.

Lawton, T. J., & Bradford, B. A. (2011). Correlation and provenance of upper Cretaceous (Campanian) fluvial strata, Utah, U.S.A., from zircon U-Pb geochronology and petrography. *Journal of Sedimentary Research*, *81*, 495–512.

Lindsey, D. A. (1998). Laramide structure of the central Sangre de Cristo Mountains and adjacent Raton Basin, southern Colorado. *Mountain Geologist*, *35*(2), 55–70.

Lipman, P. W., Steven, T. A., & Mehnert, H. H. (1970). Volcanic history of the San Juan Mountains, Colorado, as indicated by potassium-argon dating. *Geological Society of America Bulletin*, *81*, 2329–2352. https://doi.org/10.1130/0016-7606(1970)81[2329:VHOTSJ]2.0.CO;2

Lisenbee, A. L. (2013). Multi-stage Laramide deformation in the area of the southern Santa Fe embayment (Rio Grande rift), north-central New Mexico. *Geological Society of America Special Papers*, *494*, 239–260.

Liu, L., & Gurnis, M. (2010). Dynamic subsidence and uplift of the Colorado Plateau. *Geology*, *38*(7), 663–666. https://doi.org/10.1130/G30624.1

Liu, L., Gurnis, M., Seton, M., Saleeby, J., Müller, R. D., & Jackson, J. M. (2010). The role of oceanic plateau subduction in the Laramide orogeny. *Nature Geoscience*, *3*, 353–357. https://doi.org/10.1038/ngeo829

Liu, S., & Currie, C. A. (2016). Farallon plate dynamics prior to the Laramide orogeny: Numerical models of flat subduction. *Tectonophysics*, *666*(Suppl. C), 33–47. https://doi.org/10.1016/j.tecto.2015.10.010

Logsdon, M. J. (1981). A preliminary basin analysis of the El Rito Formation (Eocene), north-central New Mexico. *Geological Society of America Bulletin*, *92*(12), 968–975. https://doi.org/10.1130/0016-7606(1981)92<968:APBAOT>2.0.CO;2

Loring, A. K., & Armstrong, D. G. (1980). Cambrian-Ordovician syenites of New Mexico, part of a regional alkali intrusive episode. *Geology*, *8*, 344–348.

Loucks, R. G., Dodge, M. M., & Galloway, W. E. (1986). Controls on porosity and Permeability of hydrocarbon reservoirs in lower Tertiary sandstones along the Texas gulf coast. *Bureau of Economic Geology Report of Investigations*, *149*, 1–68.

Lucas, S. G. (1982). Vertebrate paleontology, stratigraphy, and biostratigraphy of Eocene Galisteo Formation, north-central New Mexico. *New Mexico Bureau of Mines & Mineral Resources Circular*, *186*, 1–34.

Lucas, S. G. (1984). Correlation of Eocene rocks of the northern Rio Grande rift and adjacent areas–Implications for Laramide tectonics. *New Mexico Geological Society Fall Field Conference Guidebook*, 35th Annual, 123–128.

Lucas, S. G., & Ingersoll, R. V. (1981). Cenozoic continental deposits of New Mexico: An overview. *Geological Society of America Bulletin*, *92*(12), 917–932. https://doi.org/10.1130/0016-7606(1981)92<917:CCDONM>2.0.CO;2

Lucas, S. G., & Williamson, T. E. (1993). Eocene vertebrates and late Laramide stratigraphy of New Mexico. *New Mexico Museum of Natural History and Science Bulletin*, *2*, 145–158.

Lucas, S. G., Cather, S., Abbott, J., & Williamson, T. (1997). Stratigraphy and tectonic implications of Paleogene strata in the Laramide Galisteo Basin, north–central New Mexico. Rio Grande Rift (Northern New Mexico). *New Mexico Geology*, *19*(4), 89–95.

Mackey, G. N., Horton, B. K., & Milliken, K. L. (2012). Provenance of Paleocene-Eocene Wilcox Group, western Gulf of Mexico basin: Evidence for integrated drainage of the southern Laramide Rocky Mountains and Cordilleran arc. *Geological Society of America Bulletin*, *124*(5/6), 1007–1024.

Maldonado, F. (2008). *Geologic Map of the Abiquiu Quadrangle*, Scientific Investigation Map 2998, United States Geological Survey, Rio Arriba County, New Mexico.

Maldonado, F., & Kelley, S. A. (2009). Revisions to the stratigraphic nomenclature of the Abiquiu Formation, Abiquiu and contiguous areas, north-central New Mexico. *New Mexico Geology*, *31*, 1.

McCarley, A. B. (1981). Metamorphic terrane favored over Rocky Mountains as source of Claiborne Group, Eocene, Texas coastal plain. *Journal of Sedimentary Petrology*, *51*, 1267–1276. https://doi.org/10.1306/212F7E82-2B24-11D7-8648000102C1865D

McMillan, N. J., & McLemore, V. T. (2001). Cambrian-Ordovician magmatism and extension in New Mexico and Colorado. *New Mexico Bureau of Geology and Mineral Resources Bulletin*, *160*, 1–11.

Miall, A. D. (1978). Lithofacies types and vertical profile models in braided river deposits: A summary. In A. D. Miall (Ed.), *Fluvial sedimentology* (Vol. *5*, pp. 597–604). Alberta, Canada: Canadian Society of Petroleum Memoir.

Nie, J., Stevens, T., Rittner, M., Stockli, D., Garzanti, E., Limonta, M., … Pan, B. (2015). Loess Plateau storage of Northeastern Tibetan Plateau-derived Yellow River sediment. *Nature Communications*, *6*, 8511. https://doi.org/10.1038/ncomms9511

Paces, J. B., & Miller, J. D. (1993). Precise U-Pb ages of Duluth complex and related mafic intrusions, northeastern Minnesota: Geochronological insights to physical, petrogenetic, paleomagnetic, and tectonomagmatic processes associated with the 1.1 Ga midcontinent rift system. *Solid Earth*, *Journal of Geophysical Research*, *98*(B8), 13997–14013. https://doi.org/10.1029/93JB01159

Park, H., Barbeau, D. L. Jr., Rickenbaker, A., Bachmann-Krug, D., & Gehrels, G. (2010). Application of foreland basin detrital-zircon geochronology to the reconstruction of the Southern and Central Appalachian Orogen. *The Journal of Geology*, *118*(1), 23–44. https://doi.org/10.1086/648400

Pillmore, C., & Flores, R. (1990). Cretaceous and Paleocene rocks of the Raton Basin, New Mexico and Colorado; stratigraphic-environmental framework: Tectonic development of the southern Sangre de Cristo Mountains, New Mexico. *New Mexico Geological Society Guidebook*, *41*, 333–336.

Press, W. H. (2007). *Numerical recipes, in the art of scientific computing* (3rd ed.). Cambridge, UK: Cambridge University Press.

Prothero, D. R., & Lucas, S. G. (1996). Magnetic Stratigraphy of the Duchesnean Part of the Galisteo Formation, New Mexico. In D. R. Prothero & R. J. Emry (Eds.), *The Terrestrial Eocene-Oligocene Transition in North America* (pp. 200–205). Cambridge, UK: Cambridge University Press.

Rasmussen, D. M., & Foreman, B. Z. (2017). Provenance of lower Paleogene strata in the Huerfano Basin: Implications for uplift of the Wet Mountains, Colorado, U.S.A. *Journal of Sedimentary Research*, *87*, 579–593. https://doi.org/10.2110/jsr.2017.30

Raynolds, R. G. (2002). Upper Cretaceous and Tertiary stratigraphy of the Denver basin, Colorado. *Rocky Mountain Geology*, *37*(2), 111–134.

Saylor, J. E., & Sundell, K. E. (2016). Quantifying comparison of large detrital geochronology data sets. *Geosphere*, *12*(1), 203–220. https://doi.org/10.1130/GES01237.1

Schoene, B., & Bowring, S. A. (2006). U-Pb systematics of the McClure Mountasin syenite: Thermochronological constraints on the age of the 40Ar/39Ar standard MMhb. *Contributions to Mineraal Petrology*, *151*, 615–630. https://doi.org/10.1007/s00410-006-0077-4

Schumm, S. A. (1981). Evolution and response of the fluvial system, sedimentologic implications. *Society of Economic Paleontologists and Mineralogists Special Publications*, *31*, 19–29.

Sharman, G. R., Covault, J. A., Stockli, D. F., Wroblewski, A.-J., & Bush, M. A. (2016). Early Cenozoic drainage reorganization of the United States Western Interior-Gulf of Mexico sediment routing system. *Geology*, *45*(2), 187–190. https://doi.org/10.1130/G38765.1

Shaulis, B., Lapen, T. J., & Toms, A. (2010). Signal linearity of an extended range pulse counting detector: Applications to accurate and precise U-Pb dating of zircon by laser ablation quadrupole ICP-MS. *Geochemistry, Geophysics, Geosystems*, *11*, 1–12. https://doi.org/10.1029/2010GC003198

Sláma, J., Košler, J., Condon, D. J., Crowley, J. L., Gerdes, A., Hanchar, J. M., … Whitehouse, M. J. (2008). Plešovice zircon—a new natural reference material for U-Pb and Hf isotopic microanalysis. *Chemical Geology*, *249*(1), 1–35. https://doi.org/10.1016/j.chemgeo.2007.11.005

Smith, G. A., Larsen, D., Harlan, S. S., McIntosh, W. C., Erskine, D. W., & Taylor, S. (1991). A tale of two volcaniclastic aprons: Field guide to the sedimentology and physical volcanology of the Oligocene Espinaso Formation and Miocene Peralta Tuff, north-central New Mexico. *New Mexico Bureau of Mines and Mineral Resources Bulletin*, *137*, 87–103.

Smith, L. N. (1992). Stratigraphy, sediment dispersal and paleogeography of the lower Eocene San Jose Formation, San Juan Basin, New Mexico and Colorado. *New Mexico Geological Society Guidebook*, 43rd Field Conference, San Juan Basins IV, 297–309.

Smith, M. E., Carroll, A. R., Jicha, B. R., Cassel, E. J., & Scott, J. J. (2014). Paleogeographic record of Eocene Farallon slab rollback beneath western North America. *Geology*, *42*(12), 1039–1042. https://doi.org/10.1130/g36025.1

Soister, P. E., & Tschudy, R. H. (1978). Eocene rocks in the Denver basin. In J. D. Pruit & P. E. Coffin (Eds.), *Energy resources of the Denver basin* (pp. 231–235). Denver, CO: Rocky Mountain Association of Geologists.

Stacey, J. S., & Kramers, J. (1975). Approximation of terrestrial lead isotope evolution by a two-stage model. *Earth and Planetary Science Letters*, *26*(2), 207–221. https://doi.org/10.1016/0012-821X(75)90088-6

Stearns, C. E. (1943). The Galisteo Formation of north-central New Mexico. *The Journal of Geology*, *51*(5), 301–319. https://doi.org/10.1086/625156

Stearns, C. E. (1953). Upper Cretaceous rocks of Galisteo-Tonque area, north-central New Mexico. *American Association of Petroleum Geologists Bulletin*, *37*(5), 961–974.

Stephens, M. A. (1970). Use of the Kolmogorov-Smirnov, Cramer-Von Mises, and related statistics without extensive tables. *Journal of the Royal Statistical Society*, *Series B*, 115–122.

Sundell, K. E., & Saylor, J. E. (2017). Unmixing detrital geochronology age distributions. *Geochemistry, Geophysics, Geosystems*, *18*, 1–15. https://doi.org/10.1002/2016GC006774

Sundell, K. E. (2017). U-Pb Toolbox at the University of Houston: An open-source program for reducing and visualizing zircon U-Pb data sets. *Computers & Geosciences* (Ph.D. thesis). University of Houston, Houston, TX.

Tarduno, J. A., McWilliams, M., Debiche, M. G., Sliter, W. V., & Blake, M. C. (1985). Franciscan Complex Calera limestones: Accreted remnants of Farallon Plate oceanic plateaus. *Nature*, *317*, 345–347. https://doi.org/10.1038/317345a0

Todd, T. W., & Folk, R. L. (1957). Basal Claiborne of Texas, record of Appalachian tectonism during Eocene. *American Association of Petroleum Geologists Bulletin*, *41*, 2545–2566.

Wahl, P. J., Yancey, T. E., Pope, M. C., Miller, B. V., & Ayers, W. B. (2016). U-Pb detrital zircon geochronology of the Upper Paleocene to Lower Eocene Wilcox Group, east-central Texas. *Geosphere*, *12*(5), 1517–1531. https://doi.org/10.1130/GES01313.1

Weil, A. B., & Yonkee, A. (2012). Layer-parallel shortening across the Sevier fold-thrust belt and Laramide foreland of Wyoming: Spatial and temporal evolution of a complex geodynamic system. *Earth and Planetary Science Letters*, *357–358*, 405–420. https://doi.org/10.1016/j.epsl.2012.09.021

Wissink, G. K., Wilkinson, B. H., & Hoke, G. D. (2018). Pirwise sample comparisons and multidimensional scaling of detrital zircon ages with examples from the North American platform, basin, and passive margin settings. *Lithosphere*, *10*(3), 478–491. https://doi.org/10.1130/L700.1.

Woodburne, M. O., & Swisher III, C. C. (1995). Land mammal high-resolution geochronology, intercontinental overland dispersals, sea levels, climate, and vicariance. *Society of Economic Paleontologists and Mineralogists, Special Paper*, *54*, 335–364.

Woodward, L. A. (1987). Geology and mineral resources of Sierra Nacimiento and vicinity, New Mexico. *New Mexico Bureau of Mines & Mineral Resources Memoirs*, *42*(84), 103–108.

Woodward, L. A., Hultgren, M. C., Crouse, D. L., & Merrick, M. A. (1992). Geometry of Nacimiento-Gallina fault system, northern New Mexico. *New Mexico Geological Society Guidebook*, 43rd Field Conference, San Juan Basin IV, 103–108.

Yin, A., & Ingersoll, R. V. (1997). A model for evolution of Laramide axial basins in the Southern Rocky Mountains, USA. *International Geology Review*, *39*(12), 1113–1123. https://doi.org/10.1080/00206819709465318

SUPPORTING INFORMATION

Additional supporting information may be found online in the Supporting Information section at the end of the article.

How to cite this article: Smith TM, Sundell KE, Johnston SN, et al. Drainage reorganization and Laramide tectonics in north-central New Mexico and downstream effects in the Gulf of Mexico. *Basin Res*. 2019;00:1–34. https://doi.org/10.1111/bre.12373